SLAC-PUB-1614
July 1975
(T/E)

LECTURES ON ELECTRON-POSITRON ANNIHILATION -- PART I

THE PRODUCTION OF HADRONS AND ψ PARTICLES

Martin L. Perl

Stanford Linear Accelerator Center
Stanford University
Stanford, Calif.

This is the first part of a series of tutorial lectures delivered at the Institute of Particle Physics Summer School, McGill University, June 16-21, 1975.

The two parts have separately numbered equations and references.

Table of Contents -- Part I

1. GENERAL THEORY

1.1 Introduction

Although the study of high energy electron-positron annhilation is one of the newest areas in elementary particle physics, a wide range of experimental knowledge has already been acquired--tests of quantum electrodynamics, measurements of the total cross section for hadron production, studies of inclusive reactions, the discovery of the ψ particles and the elucidation of their properties, searches for anomalous lepton production, are examples. It is no longer possible to discuss all of these topics in a series of lectures. Therefore I am going to restrict my discussions in two ways. First, the energy range under discussion will be restricted to center-of-mass energies above 2. GeV. Hence the very interesting region of vector meson production and transition to the continuum will not be considered. Second, I will only discuss the last four topics listed above: total cross section for hadron production, inclusive reaction distributions, properties of the ψ particle, and anomalous lepton production.

Much of the data which I will discuss was acquired by the SLAC-LBL magnetic detector collaboration[1] using the SPEAR colliding beams facility at the Stanford Linear Accelerator Center. Other, very important, data comes from the ADONE facility at Frascati[2], the DORIS facility at DESY, and from the colliding beams research done at the Cambridge Electron Accelerator. My restriction to higher energies prevents the discussion of the extensive research done at Orsay[3] and Novosibirsk[4].

To keep these printed notes to manageable length, the printed text will be brief. Much of the first few lectures is extracted from a longer review paper by G. Feldman and myself[5]. The reader is referred to that paper for a much fuller discussion.

1.2 General Dynamics and Kinematics

The most general process for the production of hadrons in $e^+ - e^-$ annihilations is shown in Fig. 1a. Here the cross hatched region might include a direct electron-hadron interaction. But existing data do not demand such an interaction. And if we accept the traditional belief that the electron has only electromagnetic and weak interactions, the dominant process is the exchange of a single, timelike virtual photon between the electronic and the hadronic systems, Fig. 1b. Higher order photon exchange processes, Fig. 1c, may also occur. Although such processes are expected to have cross sections smaller by a factor of the order $\alpha = 1/137$ compared to the single photon exchange process there is no experimental evidence on this point.

Returning to the single photon exchange process, Fig. 1b, we see that all the ignorance hidden in the cross hatched region of the diagram in Fig. 1a has been transferred to the photon-hadron vertex. The basic problem is to find the correct dynamical description of that vertex.

In the simplest colliding beams situation, the electron and positron have equal, but opposite, momenta in the laboratory system, Fig. 2a. Then the laboratory and center-of-mass system coincide. Designating the energy of each beam by E, we have

$$W = 2E \tag{1-1}$$

where W is the total energy of the hadronic system. We also use

$$s = W^2 = 4E^2 \quad ; \tag{1-2}$$

s is of course also the square of the four-momentum of the timelike virtual photon in Fig. 1b. We note that we use a metric in which the product of two four-vectors is given by $a \cdot b = a^\mu b_\mu = a^0 b^0 - \underset{\sim}{a} \cdot \underset{\sim}{b}$. When the angle between the two beams, η, is non-zero, Fig. 2b, we have (ignoring the electron mass)

$$s = 2E^2(1 + \cos \eta) \tag{1-3}$$

For the general reaction

$$e^+ + e^- \rightarrow 1 + 2 + 3 + \qquad (1\text{-}4)$$

in which N particles designated by 1, 2, 3 ... N are produced, the cross section is[6,7]

$$\sigma = \frac{8\pi^4}{s} \sum_{\substack{e^+,e^- \text{ spins} \\ \text{final spins}}} \int \prod_{n=1}^{N} \left(\frac{d^3 p_n}{(2\pi)^3 \, 2E_n} \right) |T_{fi}|^2 \; \delta^4(P_f - P_i) \qquad (1\text{-}5)$$

As usual the summation over spins means an average over the initial states and a summation over the final states. Here, as in the remainder of this paper, we set the electron mass equal to zero. This and all formulas in this paper are in the center-of-mass frame.

Assuming one-photon exchange, Fig. 1b, the matrix element T_{fi} has the form

$$T_{fi} = \frac{-e^2 \, j^{\mu}_{e^+e^-} \, J_{had,\,\mu}}{s} \qquad (1\text{-}6)$$

$j_{e^+e^-}$ is the leptonic transition current and J_{had} is the four-vector transition current between the vacuum and the final state particles.

In the center-of-mass system, taking the e^+ to be moving along the +z axis and the beams to be unpolarized we obtain a useful simplification of Eqs. 1-5 and 1-6. Noting that the virtual photon four-momentum k has the properties

$$k = (k^0, \underset{\sim}{k}), \; \underset{\sim}{k} = 0 \quad , \quad k^0 = W \quad , \quad k^{\nu} \, J_{had,\nu} = 0 \qquad (1\text{-}7a)$$

we obtain

$$J_{hadron,0} = 0 \qquad (1\text{-}7b)$$

and

$$\sigma = \frac{(2\pi)^6 \alpha^2}{s^2} \sum_{\substack{\text{final}\\ \text{spins}}} \int \prod_{n=1}^{N} \left(\frac{d^3 p_n}{(2\pi)^3 \, 2E_n} \right) \left[J^{\dagger}_{had,x} J_{had,x} + J^{\dagger}_{had,y} J_{had,y} \right]$$

$$\times \, \delta^4(P_f - P_i) \tag{1-8}$$

The subscripts x and y on J_{had} refer to the x and y spatial axis.

We note that the order of magnitude of the cross section is set by α^2; $\alpha = 1/137$ is the electromagnetic coupling constant. Furthermore, unless the integral over the current increases with energy, the cross section will decrease at least as rapidly as $1/s^2$ as s increases.

The acceptance of single photon exchange as the dominant process also leads to a strong restriction on the angular distribution of the entire hadronic system because the total angular momentum of the hadronic system is 1. The angular distribution is limited to the terms 1, $\sin\theta$, $\cos\theta$, $\sin^2\theta$, $\cos^2\theta$, $\sin\theta\cos\theta$ with respect to θ; and to 1, $\sin\varphi$, $\cos\varphi$ with respect to φ (θ, φ being the spherical angles about the z axis). If the e^+ and e^- beams are unpolarized, as in Eq. 1-8, there will be no φ dependence.[8] For the remainder of this paper we shall ignore polarization effects.

A few examples will illustrate these points. Consider first, just two pseudoscalar particles in the final state, Fig. 3a, such as

$$e^+ + e^- \rightarrow \pi^+ + \pi^- \tag{1-9a}$$

or

$$e^+ + e^- \rightarrow K^+ + K^- \tag{1-9b}$$

Then for Eq. 1-9a

$$\frac{d\sigma_{\pi^+\pi^-}}{d\Omega} = \frac{\alpha^2 \beta^3 \sin^2\theta \, |F_\pi(s)|^2}{8s} \tag{1-10}$$

and a similar equation holds for E. 1-9b. Here $\beta = m/E$ where m is the mass of the π. $F_\pi(s)$ is the pion form factor.[6] The total cross section is

$$\sigma_{\pi^+\pi^-} = \frac{\pi\alpha^2\beta^3|F_\pi(s)|^2}{3s} \tag{1-11}$$

As another example consider the production of just two spin 1/2 <u>point</u> Dirac particles; the only known example being (Fig. 3b)

$$e^+ + e^- \rightarrow \mu^+ + \mu^- \tag{1-12}$$

Then

$$\frac{d\sigma_{\mu\mu}}{d\Omega} = \frac{\alpha^2\beta}{4s}\left[(1 + \cos^2\theta) + (1 - \beta^2)\sin^2\theta\right] \tag{1-13a}$$

In the high energy limit of $\beta \rightarrow 1$

$$\frac{d\sigma_{\mu\mu}}{d\Omega} = \frac{\alpha^2(1 + \cos^2\theta)}{4s} \tag{1-13b}$$

$$\sigma_{\mu\mu} = \frac{4\pi\alpha^2}{3s} = \frac{21.71}{E^2}\ \text{nb} \quad ;\ E \text{ in GeV} \tag{1-13c}$$

One-photon exchange leads to the following restrictions on the final state

(a) The final state parity (P) = -1 since parity is conserved in electromagnetic interactions.

(b) The final state isotopic spin (I) is 0 or 1 on the usual assumption that the photon couples almost exclusively to I = 0 or I = 1 states.

(c) The final state charge conjugation number (C) is -1. This prohibits the reaction $e^+ + e^- \rightarrow \pi^0 + \pi^0$, although the reaction is allowed in the two-photon exchange process Fig. 1.c.

(d) If the final state contains only pions, then the G-parity relation, $G = C(-1)^I$, demands[9]

odd number of pions if I = 0
even number of pions if I = 1 (1-14)

1.3 The Parton Model

In the parton model of hadron production we think of the photon-hadron vertex as a two step process, Fig. 4,

$$e^+ + e^- \rightarrow \text{parton} + \text{antiparton} \tag{1-15}$$

$$\text{parton} + \text{antiparton} \rightarrow \text{hadrons} \tag{1-16}$$

The attractive part of this model is that it makes definite predictions about the size and energy dependence of the total cross section for hadron production, $\sigma_{had}(s)$, if we assume:

1. The partons are point particles with form factors equal to unity.

2. There are a fixed number of kinds of partons with set spins and charges.

3. Free partons cannot exist. Hence every parton-antiparton pair which is produced has a probability of 1 of going into a hadronic final state.

For a parton of mass m, spin 1/2 and charge Qe, e being the unit electric charge, the model predicts

$$\sigma_{had}(s) = \frac{4\pi\alpha^2 Q^2}{3s}, \qquad m \ll \sqrt{s/4} \tag{1-17}$$

If the parton mass m, is close to $\sqrt{s/4}$ we expect that threshold effects will lead to a cross section less than that in Eq. 1-17 When m is much greater than $\sqrt{s/4}$, we expect the cross section to be much smaller, although virtual parton pairs can still contribute. If there are N

types of partons, type n having charge $Q_n e$, all with sufficiently small mass; then

$$\sigma_{had}(s) = \frac{4\pi\alpha^2 R}{3s} \qquad (1\text{-}18\ )$$

where (for spin 1/2 partons)

$$R = \sum_{n=1}^{N} Q_n^2 \qquad (1\text{-}19a)$$

For later use we note that the numerical form of Eq. 1-18b is

$$\sigma_{had}(s) = \frac{21.71R}{E^2}\ \text{nb} \qquad (1\text{-}18\ )$$

where E is the electron or positron energy in GeV.

The significance of Eq. 1-18 is simple. The α^2 comes from the electromagnetic coupling constant at each end of the photon line; the $1/s$ comes from the $1/s^2$ contribution of the photon propagator to the cross section, a power of s being cancelled by vector coupling of the photon. One might argue that most of Eqs. 1-18 is simply a result of one-photon exchange, the significant contribution of the parton model being solely to set the magnitude of R.

Indeed the magnitude of R is so important that R has become an experimental as well as theoretical quantity in its own right. It has become conventional to note Eq. 1-18 is just R times the equation for the cross section of the reaction $e^+ + e^- \rightarrow \mu^+ + \mu^-$ (Eq. 1-13c) when the muon mass is neglected. We define

$$R(s) = \frac{\sigma_{had}(s)}{\sigma_{\mu\mu}(s)} \qquad (19b)$$

Of course the basic questions are: do partons exist; and if so do they have unit form factors, what are their spins, what are their charges?

The conventional phenomenology is that there are at least three types of quark-partons — the u, d, and s quark with the properties given in Table I. We use the term quark-partons to denote partons with specific spin and internal quantum numbers. If only these quark-partons exist

$$R_{uds} = (2/3)^2 + (1/3)^2 + (1/3)^2 = 2/3 \qquad (1\text{-}20a)$$

As we shall see in Sec. 3, the pure quark-parton model fit to the total cross section requires R in the range 3 to 5. Some increase in R can be obtained by accepting the existence of a fourth quark — the charm[10] carrying quark (c) — which has Q = 2/3 (see Table I). Then

$$R_{udsc} = 10/9 \quad ; \qquad (1\text{-}20b)$$

but this is not much of an increase.

To obtain R in the 3 to 5 range we obviously need many more fractional charged quark-partons or integrally charged partons. The first alternative is illustrated by the colored quark-parton scheme.[10] Here an additional three-valued quantum number called color — red, white, and blue — is postulated. Then there are three different u quarks, 3 different d quarks and so forth. Thus

$$R_{uds,color} = 2 \quad , \quad R_{udsc,color} = 10/3 \qquad (1\text{-}20c)$$

The integral charge parton scheme is illustrated by the Han and Nambu model.[10] This model contains 9 quarks, 4 have charge $\pm$ 1 and 5 have charge 0. Thus

$$R_{Han\text{-}Nambu} = 4 \qquad (1\text{-}20d)$$

Even if we do not accept a parton model of $e^+ - e^-$ annihilations very general light cone arguments[11,12] lead to the same s dependence

for σ_{had} as is given by Eq. 1-18 namely

$$\sigma_{had}(s) = \frac{\text{constant}}{s} \tag{1-21}$$

for sufficiently large s.

1.4 The Vector Meson Dominance Model

In the vector meson dominance model,[13-15] Fig. 5, the photon couples at the vertex marked $G_{\gamma V}(s)$ to a vector meson resonance, V, such as the ρ^0, ω or φ. The hadronic final states are then simply the decay modes of the V. Of course for a hypothetical high mass vector meson we know nothing a priori about its decay modes — hence the cross hatched area in Fig. 5, once again showing our ignorance. However if we are willing to make an assumption about $G_{\gamma V}(s)$ we can calculate the total hadronic cross section. Indeed we assume $G_{\gamma V}$ is a constant. Then σ_{tot} is described by a simple Breit-Wigner resonance, which in its relativistic form is

$$\sigma_{had}(s) = \frac{12\pi M_V^2 \, \Gamma_{ee} \, \Gamma_V}{s\left[(s - M_V^2)^2 + M_V^2 \Gamma_V^2\right]} \tag{1-22a}$$

here M_V is the resonance mass, Γ_V is the full width, and Γ_{ee} is the partial width for the decay

$$V \rightarrow e^+ + e^- \tag{1-23}$$

given by

$$\Gamma_{ee} = \frac{\alpha^2 \, M_V}{3(g_V^2/4\pi)} \tag{1-24}$$

Finally $g_V^2/4\pi$ is a measure of the γ-V coupling; explicitly

$$G_{\gamma V}^2 = \frac{\alpha}{(g_V^2/4\pi)} \tag{1-25}$$

Thus the larger g_V, the weaker the γ-V coupling — a rather unfortunate convention. An alternative form for σ_{had} is

$$\sigma_{had}(s) = \frac{4\pi\alpha^2 M_V^3 \Gamma_V}{(g_V^2/4\pi)\ s\left[(s - M_V^2)^2 + M_V^2\ \Gamma_V^2\right]} \tag{1-22b}$$

At $s = M_V^2$

$$\sigma_{had,max} = \frac{12\pi}{s}\ \frac{\Gamma_{ee}}{\Gamma_V} = \frac{4\pi\alpha^2}{(g_V^2/4\pi)M_V\Gamma_V} \tag{1-22c}$$

Values of M_V, Γ_V, Γ_{ee} and $g_V^2/4\pi$ for the well known vector mesons are given in Table II.

If there is a mass M_{max} such that <u>all</u> vector mesons have $M_V < M_{max}$, than unless the higher energy tails of the resonance have a form other than that given by Eq. 1-22a

$$\sigma_{had}(s) = \text{constant}/s^3 \quad ; \quad \text{for } s >> M_{max} \tag{1-26}$$

On the other hand we may postulate an infinite series of vector mesons with ever increasing mass. Thus we may have a slower dependence on s.

$$s_{had}(s) \geqslant \text{constant}/s^n, \quad n < 3 \quad ; \quad \text{as } s \to \infty \tag{1-27}$$

This is obvious. It is also obvious that by adjusting the magnitude of g_V and the mass spectrum of the V's, one can obtain any desired R.

1.5 The Statistical Model for Final States

Assuming one-photon exchange, one might expect the final states in electron-positron annihilation to be at least partially described by

statistical model considerations ; or at least to be better described by such models than are the final states produced in hadron-hadron collisions. Hadron-hadron collisions are dominated by peripheral effects which produce a strong anisotrophy in the center-of-mass. Most particles move in the forward or backward direction along the line of collisions. However in electron-positron annihilation through one-photon exchange there is center-of-mass isotropy except for the spin 1 effects discussed in Sec. 1.2. And from a more dynamic point of view, the electron-positron annihilation may be regarded as the formation of a single fireball of energy. The decay of that fireball providing an excellent situation for using statistical ideas.

Returning to Fig. 1b we apply the Fermi statistical model[6,17] first to the simplified case in which N identical spin 0 hadrons are produced in the final state. To evaluate the $J^{\dagger}J$ term in Eq. 1-8 we follow Fermi and assume that the energy of the annihilation is contained in a volume Ω. The fundamental assumption is that for N particles in the final state, $J^{\dagger}J$ is proportional to the probability of finding N particles in the volume Ω. Since our normalization convention is that a particle of energy E has a particle density of 2E per unit volume; explicitly

$$J^{\dagger}_{had}J_{had} = A\prod_{n=1}^{N}(2E_n\Omega) \tag{1-28}$$

where A is a proportionality constant. Equation 1-8 becomes:

$$\sigma_N = \frac{(2\pi)^6\alpha^2 A}{s^2 N!}\int\prod_{n=1}^{N}\left[\left(\frac{E_n\Omega}{(2\pi)^3}\right)\frac{d^3p_n}{E_n}\right]\delta^4(P_f - P_i) \tag{1-29}$$

The N! appears in the denominator because there are N identical particles. Following modern treatments[6] of the statistical model we replace the term $E_n\Omega/(2\pi)^3$ by its average value, $1/s_0$, and we retain the Lorentz invariant phase space factors d^3p_n/E_n. Hence

$$\sigma_N(s) = \frac{(2\pi)^6\alpha^2 A}{s^2 N!} \frac{1}{s_0^N} \int \prod_{n=1}^{N} \left(\frac{d^3p_n}{E_n}\right) \delta^4(P_f - P_i) \tag{1-30a}$$

and

$$\sigma_{had}(s) = \sum_{n=2}^{\infty} \sigma_N(s) \tag{1-30b}$$

Equations 1-30 predict the energy dependence of the total and topological cross sections, the multiplicity distributions, and the momentum distributions. For example if the particles have zero mass the multiple integral in Eq. 1-30a can be evaluated analytically.[6] Then

$$\int \prod_{n=1}^{N} \left(\frac{d^3p_n}{E_n}\right) \delta^4(P_f - P_i) = \frac{2\pi^{N-1}\, s^{N-2}}{(N-1)!\ (N-2)!} . \tag{1-31}$$

and

$$\sigma_N(s) = \frac{\alpha^2 B}{N!\,(N-1)!\ (N-2)!} \left(\frac{s}{s_0'}\right)^{N-4} \tag{1-32}$$

Here $B = 2(2\pi)^6 A/(\pi s_0'^4)$ and $s_0' = s_0/\pi$ are constants. This simple model can yield momentum and multiplicity distributions which crudely fit the data. But it cannot give the correct energy behavior. The partial cross sections increase as powers of s for $N > 4$, yet the data (Sec. 3) show that the total cross section ultimately decreases as s increases.

This is of course a basic problem of this model.

Therefore for actual use in studying $e^+ - e^-$ annihilations we retain only the Lorentz invariant phase space aspects of the model, allowing the matrix element $J^\dagger J$ to be extracted as an arbitrary function of (s). Explicitly we replace Eq. 1-30a by

$$\sigma_N(s) = C_N(s) \int \prod_{n=1}^{N} \left(\frac{d^3 p_n}{E_n} \right) \delta^4(P_f - P_i) \qquad (1\text{-}33)$$

Here $C_N(s)$ is an empirically determined function of s. Of course in the actual data we have not a single type of particle, but many types -- $\pi^\pm$, π^0, $K^\pm$, K^0, p, $\bar{p}$ and so forth. Equation 1-33 must therefore be enlarged to include various kinds of particles. Also charge, strangeness, and baryon number must be conserved. The calculation of $\sigma_N(s)$ under these conditions must be done numerically.

2. COLLIDING BEAM FACILITY PARAMETERS

Colliding beams facilities are in many ways the most intricate accomplishment of the accelerator builder. And this is not the place to describe these facilities. However it is useful to survey the energy and intensity properties of existing and proposed electron-positron facilities[18,19] so that the reader can understand the present range of experimental possibilities. In an electron-positron colliding beams facility the beams move in opposite directions in either separate rings,

or in different orbits in the same ring. It is only at the interaction regions where the beam orbits intersect and where the particles may collide.

In a colliding beams facility the crucial quantities are the energy, E, of each beam defined in Sec. 1.B, and the luminosity, L. Consider the simple case in which the two beams have equal but opposite momentum. The particles in the beams are not distributed uniformly around the orbit, but collect in bunches. Suppose that a bunch is a cylinder of length ℓ cross sectional area A, and that it contains N particles. When a single electron bunch passes thru a single positron bunch, the number of events produced thru the reaction $e^+ + e^- \rightarrow X$ with cross section σ_X is $N^2\sigma_X/A$. If there are f bunch collisions per interaction region per second.

$$\text{Number } (e^+ + e^- \rightarrow X) \text{ events per second} = \frac{N^2 f \sigma_X}{A} \qquad (2\text{-}1)$$

It is therefore useful to define the luminosity, L, where

$$L = \frac{N^2 f}{A} \quad \text{cm}^{-2}\ \text{sec}^{-1}$$

Then

$$\text{number } (e^+ + e^- \rightarrow X) \text{ events per second} = L\sigma_X \qquad (2\text{-}2)$$

Existing facilities have actual luminosities in the range of 10^{29} to 10^{32} $\text{cm}^{-2}\ \text{sec}^{-1}$. Design goal luminosities for existing and proposed accelerators go as high as 10^{33} $\text{cm}^{-2}\ \text{sec}^{-1}$. To get some feeling for these quantities note that the typical total hadronic production cross section, σ_{had}, is 20 nb in the high energy region (Sec. 3). Effective luminosities of 10^{29} to 10^{31} $\text{cm}^{-2}\ \text{sec}^{-1}$ then correspond to from 7 to 700

hadronic events produced per hour.

Parameters of existing and proposed electron-positron colliding beam facilities are given in Table III.

3. TOTAL CROSS SECTION

3.1 Data

Figure 6 shows the total cross for hadronic production, σ_{had} as a function of the total energy W. We observe several kinds of energy dependence.

(a) There are the very narrow resonances, the ω, φ, $\psi(3100)$ and $\psi(3700)$ with full widths of 10 MeV or less.

(b) There are the much broader ρ^0 resonances and the broad resonance-like structure at 4.1 GeV. Incidently, although the ω and ρ^0 appear superimposed in this total cross section curve, they are easily separated experimentally; the dominant decay modes being $\rho^0 \rightarrow \pi^+ + \pi^-$ and $\omega \rightarrow \pi^+ + \pi^- + \pi^0$ respectively (Table II).

(c) Between the resonances is the continuum region which itself has an energy dependence — broadly speaking in the continuum region σ_{had} decreases as W increases.

The higher energy data displayed in Fig. 6 are listed in Table IV along with references.[20-27]

3.2 Interpretation

As I stated in the Introduction I am restricting my discussion to center-of-mass energies above 2 GeV

To simplify the discussion of this region I postpone consideration of the ψ particles to Sec. 6. With the ψ particles removed, σ_{had} (Figs. 6 and7a) shows a roughly monotonic decrease from above 40 nb at 2 GeV to about 10 nb in the 7 GeV range. The only presently known exception to this decrease is a broad enhancement at 4.1 GeV. If we draw a straight line between the 3.8 and 4.8 GeV data points, we obtain for this object

Center ~ 4.1 GeV
Height above smooth σ_{had} ~ 12 nb
Full width at half maximum height ~ 240 MeV

The nature of this enhancement — in particular, is it a resonance — is discussed in Ref. 5.

To study the energy dependence of σ_{had} we use R defined in Eq. 1-18 R is listed in Table IV and shown in Fig. 7b. We recall that if R is a constant, σ_{had} varies as 1/s. There is a sequence of observations which can be made on these data.

(a) R is approximately constant at a value of 2.5 from 2 to about 3.5 GeV. To within 25%, this behavior agrees with that expected from the parton model for three colored quarks (Eq. 1-20c).

(b) R increases dramatically as W goes from 3.5 to 5 GeV with most of the increase occurring rather suddenly in the neighborhood of 4 GeV. The increase in R is

$$\Delta R = \langle R \rangle_{4 \text{ to } 5 \text{ GeV}} - \langle R \rangle_{3 \text{ to } 4 \text{ GeV}} =$$

2.2 ± 0.2 including 4.1 GeV enhancement
1.6 ± 0.2 excluding 4.1 GeV enhancement

Thus the increase occurs whether or not we include the 4.1 GeV enhancement. The fascinating and as yet unanswered question is whether the 4.1 GeV enhancement has anything to do with the increase in R.

One possible explanation is that as W increases above 4 GeV, a new set of higher mass quark-partons contributes to hadron production through the diagram in Fig. 4. Labeling these partons by $n = N + 1$, $N + 2 \ldots N'$; the increase in R, Eq. 1-19a, would simply come from

$$\Delta R = \sum_{n=N+1}^{N'} Q_n^2 .$$

In this picture the 4.1 GeV enhancement could be either a threshold effect, or a resonance, or a combination of both.

(c) Above 5 GeV, R either remains constant or slowly increases; the errors are large. The important point is that there is absolutely <u>no</u> indication that R is beginning to decrease in this highest energy region. Hence any theory which requires R to be much smaller than 5--Eqs.1-20a through 1-20c, for example-- is either wrong or applies to a yet higher energy region. If the latter explanation is used, one must explain why energies of the order of 6 or 7 GeV are still in a transition region.[28]

(d) An alternate way out of the large R problem is to assume that one or more heavy leptons or elementary bosons begin to be produced in pairs in the 4 to 5 GeV region. Each new type of heavy lepton would contribute one unit of R. The contribution from an elementary boson is less definite--it depends upon assumptions as to the magnetic and higher moments. This is discussed in Part II of these lectures.

4. MULTIPLICITIES

4.1 Charged Particle Multiplicities

The average charged particle multiplicity, $< N_{ch} >$, is given in Table IV and Fig. 8. As shown in Fig. 8 we can fit $< N_{ch} >$ by the simple equation

$$< N_{ch} > = a + b\ln(W) \quad ; \; a = 1.93, \; b = 1.50 \qquad (4\text{-}1).$$

There is no drastic change in $< N_{ch} >$ at the 4.1 GeV enhancement, or as R increases in the 3.5 to 4.5 GeV region.

4.2 Comparison With Multiplicities In Hadron-Hadron Collisions.

An immediate question is how does $\langle N_{ch} \rangle_{ee}$ for

$$e^+ + e^- \rightarrow \text{hadrons} \qquad (4\text{-}2)$$

compare with $\langle N_{ch} \rangle$ for

$$\begin{aligned} &\pi^{\pm} + p \rightarrow \text{hadrons} \\ &K^{\pm} + p \rightarrow \text{hadrons} \\ &p + p \rightarrow \text{hadrons} \end{aligned} \qquad (4\text{-}3)$$

The answer is given in Fig. 8 . As has been discussed by Whitmore,[29] $\langle N_{ch} \rangle$ for $\pi^- p$ and pp can be described by a single curve by defining the total initial state kinetic energy in the center-of-mass frame

$$Q = \sqrt{s} - m_a - m_b \qquad (4\text{-}4)$$

for the reaction

$$a + b \rightarrow \text{hadrons} \qquad (4\text{-}5)$$

The masses of a and b are m_a and m_b respectively. Then the single formula

$$\langle N_{ch}\rangle = 2.45 + 0.32 \ln Q + 0.53 \ln^2 Q \qquad (4\text{-}6)$$

(curve A in Fig. 8) using $W_{ee} \equiv Q$, fits both $\pi^- p$ and pp multiplicities We see that $\langle N_{ch}\rangle_{ee}$ is very similar in magnitude and W behavior to $\langle N_{ch}\rangle_{\pi^- p}$ and $\langle N_{ch}\rangle_{pp}$ when we use $W = Q$. Incidently the deviations of $\langle N_{ch}\rangle_{ee}$ from curve A are not much greater than the deviations from a universal fit to $\langle N_{ch}\rangle$ for just hadron-hadron collisions; such deviations[30] are less than $\pm$ 0.3 units in $\langle N_{ch}\rangle$.

We might also expect that $\langle N_{ch}\rangle_{ee}$ should be very similar to $\langle N_{ch}\rangle_{\bar{p}p \text{ annihilation}}$ for the reaction in Eq. 4-4. Unfortunately in higher energy $\bar{p}p$ data it is difficult to separate that reaction from the non-annihilation reaction

$$\bar{p} + p \rightarrow \text{ nucleon + antinucleon + mesons} \qquad (4\text{-}7)$$

Hence $\langle N_{ch}\rangle_{\bar{p}p}$ contains both reactions. From Abesalashvli et al.[31] we take the empirical fit.

$$\langle N_{ch}\rangle_{\bar{p}p} = 0.69 + 2.10 \ln W_{\bar{p}p} \qquad (4\text{-}8)$$

In comparing $\langle N_{ch}\rangle_{ee}$ with $\langle N_{ch}\rangle_{\bar{p}p}$ in Fig. 10b we can either set

$$W_{ee} \equiv W_{\bar{p}p} \text{ ; curve B} \qquad (4\text{-}9a)$$

or

$$W_{ee} \equiv W_{\bar{p}p} - 2M_{proton} \text{ ; curve C} \qquad (4\text{-}9b)$$

Equation 4-9a would be the correct equivalence if only $\bar{p}p$ annihilation occurred; Eq. 4-9b would be correct if no annihilation occurred. We see that the truth falls in between.

5. INCLUSIVE DISTRIBUTIONS AND SCALING

5.1 Single Particle Momentum Distributions

As we begin to study the dynamics of the final hadronic states produced in $e^+ - e^-$ annihilation, we turn to one of the simplest properties of the multi-hadronic final states — the single particle momentum distribution. We define, for charged particles,

$$z = p/p_{max} \tag{5-1a}$$

$$p_{max}^2 = (W/2)^2 - (mass_\pi)^2 \tag{5-1b}$$

where W is as usual the total energy of the hadronic system. We are going to ignore the presence of K's, p's and $\bar{p}$'s in the data unless otherwise noted. We do this partly for simplicity and partly because we can only separate these particles in the low p region. To start without any theoretical prejudices we first look at the distribution

$$F(z,W) = \frac{1}{\langle N_{ch} \rangle \ \sigma_{had}} \ \frac{d\,\sigma_{had}}{dz} \tag{5-2a}$$

Thus

$$\int_0^1 F(z,W)dz = 1 \tag{5-2b}$$

These normalized distributions in z are shown in Fig. 9 ; and the average value of p for charged particles

$$\langle p_{ch} \rangle = \int_0^1 pF(z,W)\, dz \qquad (5\text{-}3)$$

as well as $\langle z \rangle$, is shown in Fig. 10.

We observe the following:

(a) $\langle p_{ch} \rangle$ increases slowly as W increase, varying from about 400 MeV/c to about 480 MeV/c in this W range.

(b) The production of low p hadrons is greatly favored.

(c) As W increases, F(z,W) increases in the low z region, and correspondingly decreases in the high z region.

We are immediately struck by the resemblance between F(z,W) and the $p_\perp$ distributions found in the multi-hadron final states of hadron-hadron collisions. For example in p-p collisions,[29,30] (for pions and $s \lesssim 200$ GeV^2)

$$\langle p_\perp \rangle \sim (0.23 + .051 \ln \sqrt{s})\ \text{GeV/c} \qquad (5\text{-}4)$$

And $d\sigma_{had}/dp_\perp$ has a shape,[29] except possibly for the high $p_\perp$ tails, roughly like those in Fig. 9 .

5.2 Phase Space Model for Single Particle Momentum Distributions

As noted in Sec. 1.5 we can fit the single particle momentum distributions to a phase space model in which the multiplicity distributions are fixed empirically (see Ref. 5). To see how this occurs we rewrite Eq. 1-33 in the form

$$\sigma_N(s) = C_N(s)\, R_N(s) \qquad (5\text{-}5)$$

$$R_N(s) = \int \prod_{n=1}^{N} \left(\frac{d^3 p_n}{E_n} \right) \delta^4(P_f - P_i) \qquad (5\text{-}6)$$

Then for identical particles, the single particle distribution is given by

$$\frac{E\, d\sigma_{had}(s)}{d^3p} = \sum_{n=3}^{\infty} NC_N(s) R_{N-1}(s_r) \tag{5-7a}$$

where

$$s_r = (\sqrt{s} - E)^2 - p^2 \tag{5-7b}$$

As discussed in Ref. 5 the p distribution is roughly isotopic. Hence for convenience and future use we define

$$\frac{E\, d\sigma_{had}}{p^2 dp} = 4\pi G(s,p) \tag{5-8a}$$

$$\frac{d\sigma_{had}}{dp} = \frac{4\pi p^2 G(s,p)}{E} \tag{5-8b}$$

A fit to $d\sigma(s)/dp$ at W = 4.8 GeV, using a phase space model with just pions, is shown in Fig. 11. We see that the fit is quite good — equally good fits can be made for the data at other values of W. The fact that the phase space model can provide adequate fits to $d\sigma/dp$ means that we cannot hope to see incisive tests of dynamical theories of $e^+ - e^-$ annihilation in the gross features of the momentum distribution. We have to look at more detailed behavior.

5.3 Feynman Scaling

To the veteran of hadron-hadron inclusive physics, the expression in Eq. 5-8a immediately raises the question, is there Feynman scaling[6,32,33] in $e^+ - e^-$ annihilation, analogous to that in hadron-hadron collisions? In hadron-hadron inclusive physics, Feynman scaling predicts that the Lorentz invariant differential cross section

$$\frac{E\, d\sigma_{had}}{d^3p} = H(s,\ p_{\parallel},\ p_{\perp},\ \varphi) \rightarrow H(x,\ p_{\perp}) \qquad (5\text{-}9)$$

$$x = p_{\parallel}/p_{\parallel max}$$

Thus written in terms of x and $p_{\perp}$, H is independent of s. Equation 5-9 is only correct for $p \lesssim 1$ GeV/c; at higher $p_{\perp}$ there is additional s dependence.[32] Should there be Feynman scaling in $e^+ - e^-$ annihilations? If so, in Eq. 5-8a, should $G(s,p) \rightarrow G(p)$ or should $G(s,p) \rightarrow G(p/p_{max}) = G(z)$? As shown in Fig. 12 for <u>charged</u> particles

$$\frac{E\, d\sigma_{had}}{d^3p} = G(s,p) \rightarrow G(p) \qquad (5\text{-}10)$$

is a rough fit to the data; the largest deviations are a factor of two. Thus in <u>this</u> W range there is a rough Feynman scaling in p. Thus the Feynman scaling in p here is analogous to the Feynman scaling in $p_{\perp}$ in hadron-hadron collisions. Integrating Eq. 5-10 we obtain

$$\int G(s,\ p)\ d^3p = \langle W_{ch} \rangle\ \sigma_{had} \qquad (5\text{-}11)$$

where $\langle W_{ch} \rangle$ is the average total energy in charged particles. As we expect from Fig. 10 this quantity changes little in this W range.

We should reserve judgement on the significance of this Feynman scaling in p because the data presented here have a relatively small W range. The authors know of no simple, elegant explanation for the scaling. Simple arguments such as the fragmentation model[6,34] used in hadron-hadron collisions do not apply here. Indeed as W increases we might expect to see scaling versus $z = p/p_{max}$ rather than versus p for large p. A theory which predicts something close to this will be discussed in the next section.

5.4 Bjorken Scaling

It is well known[6,35-37] that the differential cross section for electron-nucleon or muon-nucleon inelastic scattering (Fig. 13a)

$$e \text{ or } \mu + n \rightarrow e \text{ or } \mu + \text{hadrons} \tag{5-13}$$

can be described by two structure functions W_1 and W_2. Neglecting the lepton mass

$$\frac{d\sigma}{dq^2 dq\cdot P} = \frac{\pi\alpha^2}{q^4 E}\left[2|q^2|\, W_1(q^2,\ q\cdot P) + (4EE' - |q^2|)\, W_2(q^2,\ q\cdot P)\right] \tag{5-14}$$

Here q and P are the four-momenta of the virtual photon and the incidental nucleon (Fig. 13a) respectively. Also

$$P\cdot q = M\nu \tag{5-15}$$

where M is the nucleon mass. The total energy of the hadronic system W_{had} is

$$W_{had}^2 = 2M\nu + M^2 + q^2 \tag{5-16}$$

In general W_1 and W_2 are allowed to be functions of q^2 and ν; but as predicted by Bjorken and demonstrated experimentally.[6,35-37]

$$MW_1(q^2,\ q\cdot P) \rightarrow F_1(\omega) \tag{5-17a}$$

$$\nu W_2(q^2,\ q\cdot P) \rightarrow F_2(\omega) \tag{5-17b}$$

$$\omega = \frac{2P\cdot q}{|q^2|} = \frac{2M\nu}{|q^2|} \tag{5-17c}$$

$$1 \leq \omega \leq \infty \tag{5-17d}$$

for

$$|q^2| \gtrsim 1(\mathrm{GeV}/c)^2 \tag{5-18}$$

$$W_{had} \gtrsim 2 \text{ GeV}$$

The behavior of W_1 and νW_2 as functions of the single scaling variable ω (Eq. 5-17c) is called Bjorken scaling. Recently this scaling has been demonstrated to hold to within 20% even for higher energy, large $|q^2|$ muon-proton inelastic scattering.[38]

Is there an analogous scaling law for $e^+ + e^-$ annihilation

$$e^+ + e^- \rightarrow \text{hadrons} \tag{5-19}$$

From a very general point of view,[11] such as light cone algebra, the analogy to Bjorken scaling is the statement, Sec. 1.3, that R is a constant in

$$\sigma_{had}(s) = \frac{4\pi\alpha^2 R}{3s} \tag{5-20}$$

We have already discussed the validity of this prediction in Sec. 3.

However if we are willing to use a parton model[39] then we can construct other analogies to Eq. 5-17. Consider the $e^+ - e^-$ annihilation

diagram in Fig. 13b in which

$$e^+ + e^- \to h + \text{anything} \quad , \quad h = \pi \text{ or } K \text{ or } n, \tag{5-21}$$

and the momentum of the h is detected. In analogy to Eqs. 5-15 to 5-17 we define

$$P_h = \text{four-momentum of h (in Eq. 5-21)} = (E_h, \underset{\sim}{p}_h) \tag{5-22}$$

$$q^2 = s = W^2 > 0$$

$$x = \frac{2P_h \cdot q}{q^2} = \frac{2E_h}{\sqrt{s}}$$

$$0 \le x \le 1$$

With θ the angle between $\underset{\sim}{p}_h$ and the $e^+ - e^-$ axis, the equation analogous to Eq. 5-14 is

$$\frac{d\sigma_{had}}{dx\, d\cos\theta} = \frac{3}{2}\sigma_{\mu\mu}\, x\beta_h \left[M_h \bar{W}_{1h}(q^2, q\cdot P_h) + \frac{x\beta_h^2}{4}\left(\frac{E_h\sqrt{s}}{M_h}\right)\bar{W}_{2h}(q^2, q\cdot P_h)\sin^2\theta \right] \tag{5-23a}$$

Here we have used

$$\sigma_{\mu\mu} = \frac{4\pi\alpha^2}{3s} \tag{5-23b}$$

to emphasize the analogy to equations in Sec. 1.3 and to Eq. 5-20. β_h is the velocity of h.

The analogy to Eqs. 5-17 is[39]

$$M_h \bar{W}_{1h}(q^2, q\cdot P_h) \rightarrow \bar{F}_{1h}(x) \tag{5-24a}$$

$$\left(\frac{E_h\sqrt{s}}{M_h}\right)\bar{W}_{2h}(q^2, q\cdot P_h) \rightarrow \bar{F}_{2h}(x) \tag{5-24b}$$

We shall call this <u>special</u> Bjorken scaling in e^+e^- annihilations, reserving the term Bjorken scaling in e^+e^- annihilations for Eq. 5-20. Equation 5-23 becomes

$$\frac{d\sigma_{had}}{dx\, d\cos\theta} = \frac{3}{2}\,\sigma_{\mu\mu}\, x\beta_h \left[\bar{F}_{1h}(x) + \frac{x\beta_h^2}{4}\,\bar{F}_{2h}(x)\sin^2\theta\right] \tag{5-25}$$

The charged pion is the only hadron for which we have sufficient data to make use of Eq. 5-25 throughout the x range. Even so we are not yet prepared to separate $\bar{F}_{1h}$ and $\bar{F}_{2h}$. Therefore we <u>ignore the low</u> x region and approximate

$$\beta \approx 1 \quad , \quad x \approx z = p/p_{max} \tag{5-26a}$$

Also as discussed in Ref. 2 the angular distribution of the charged particle is almost uniform in cos θ. With these approximations, Eq. 5-25 reduces to

$$\left(\frac{d\sigma_{had}}{dz}\right)_\pi \approx \sigma_{\mu\mu}\, z\left[3\bar{F}_{1\pi}(z) + \frac{z}{2}\,\bar{F}_{2\pi}(z)\right] \tag{5-26b}$$

This can also be written in a form to emphasize the scaling in x (now called z)

$$s\left(\frac{d\sigma_{had}}{dz}\right)_\pi = f(z)_\pi \tag{5-26c}$$

We already know that special Bjorken scaling cannot be true for all z because from Eq. 5-26c

$$\int f(z)_\pi dz \approx s\ \sigma_{had} \langle N_{ch} \rangle \tag{5-27}$$

and the right hand side of Eq. 5-27 increases with s. Nevertheless a plot of $s d\sigma_{had}/dz$ versus z is shown in Fig. 14. There is perhaps crude special Bjorken scaling in the $z \gtrsim 0.5$ region. In this region we can ignore the pion mass, and write Eq. 5-26c in the more transparent form.

$$\frac{d\sigma_{had}}{dp} \approx 2s^{-3/2}\ f(2p/\sqrt{s}) \quad ; \quad p \gg m_\pi \tag{5-28}$$

This prediction is in general quite different from the Feynman scaling in p prediction (ignoring the pion mass again) of Eq. 5-10

$$\frac{d\sigma_{had}}{dp} \approx 4\pi p\ G(p) \quad ; \quad p \gg m_\pi \tag{5-29}$$

As s increases either Eq. 5-28, special Bjorken scaling, or Eq. 5-29, Feynman scaling, must fail. (Only G(p) having the very special form $G(p) = \text{constant}/p^4$ allows both predictions to be true.)

6. The ψ's

6.1 Discovery

For convenience I shall refer to the $\psi(3095)$ as the ψ and the $\psi(3684)$ as the ψ'.

The ψ was independently discovered at SLAC[40] in the colliding beams reaction

$$e^+ + e^- \rightarrow \psi \rightarrow \text{hadrons or lepton pairs} \qquad (6\text{-}1)$$

and at BNL in the hadronic reaction[41]

$$p + \text{nucleus} \rightarrow \psi + \text{hadrons} \rightarrow e^+ + e^- + \text{hadrons} \qquad (6\text{-}2)$$

The reaction in Eq. 6-1 has been observed at other $e^+ - e^-$ colliding beams facilities.[42,43] The ψ has also been produced using neutrons[44]

$$n + \text{nucleus} \rightarrow \psi + \text{hadrons} \quad ; \qquad (6\text{-}3)$$

and using photons [45-48]

$$\gamma + \text{nucleus} \rightarrow \psi + \text{hadrons} \quad . \qquad (6\text{-}4)$$

Below 25 GeV, the reaction in Eq. 6-4 seems to be predominantly diffractive[48]

$$\gamma + \text{nucleon} \rightarrow \psi + \text{nucleon} \qquad (6\text{-}5)$$

The ψ' was also discovered at SLAC[49] in the colliding beams reaction

$$e^+ + e^- \rightarrow \psi' \rightarrow \text{hadrons or lepton pairs} \qquad (6\text{-}6)$$

$$\text{or hadrons + lepton pairs;}$$

and has also been produced at DESY.[43]

6.2 Nature of the ψ's

The basic question about the ψ particles is are they hadrons or are they a new kind of particle? By a hadron I mean a particle which has strong interactions. I will summarize present thinking on this question before discussing the detailed properties of the ψ particles.

We determine whether a particle has strong interactions by studying (A) its total cross section when it collides with other hadrons, (B) its rate of production in hadron-hadron collisions, and (C) its decay rate and decay modes.

A. Total Cross Section

We do not know at present how to directly measure $\sigma_{tot}(\psi N)$ or $\sigma_{tot}(\psi' N)$, the total cross section for a ψ or ψ' on a nucleon. For the ψ we can calculate $\sigma_{tot}(\psi N)$ using measurements of the reactions in Eqs. 6-1 and 6-5, and vector meson dominance theory.[5,45-48] The calculation is quite speculative because we have to assume that the γ-ψ coupling does not change over a range of $(3.1\ \text{GeV})^2$ in the four-momentum squared transferred from the γ to the ψ. One obtains[45] very roughly

$$\sigma_{tot}(\psi N) \sim 1\ \text{mb} \ . \tag{6-7}$$

The known hadrons have

$$\sigma_{tot} \sim 15 \text{ to } 40\ \text{mb} \quad ; \tag{6-8}$$

Also using vector meson dominance, the established vector mesons are calculated to have.

$$\sigma_{tot}(\rho^o N) = 23 \pm 3\ \text{mb} \tag{6-9a}$$

$$\sigma_{tot}(\omega N) = 24 \pm 3\ \text{mb} \tag{6-9b}$$

$$\sigma_{tot}(\varphi N) = 9 \pm 1\ \text{mb} \tag{6-9c}$$

Thus the ψ seems to have a smaller σ_{tot} by a factor of 10 or more than established hadrons. On the other hand the $\sigma_{tot}(\psi N)$ is 10 times greater than

$$\sigma_{tot}(\gamma N) \approx 0.1 \text{ mb} \quad ; \tag{6-10}$$

and much greater than weak interaction cross sections. Thus the ψ could be a hadron with its effective strong interaction coupling constant smaller than the conventional effective strong interaction coupling constant by a factor of $\sqrt{10}$ or so. Or perhaps very high energies are requried for $\sigma_{tot}(\psi N)$ to read its asymptotic value. (see below.)

We do not have the data on the ψ' to make a similar argument.

B. Production in Hadron-Hadron Collisions

At energies of the order of 250 GeV, the reaction

$$n + \text{ nucleus} \rightarrow \psi + \text{hadrons}$$

has a cross section of roughly[44]

$$\sigma_{NN}(\psi \text{ production}) \sim 10^{-31} \text{ cm}^2/\text{nucleon} \tag{6-11}$$

This is much smaller than the π production cross section

$$\sigma_{NN}(\pi \text{ production}) \gtrsim 10^{-26} \text{ cm}^2/\text{nucleon} \quad ; \tag{6-12}$$

and it is even smaller than the antinucleon or hyperon production cross section

$$\sigma_{NN}(\bar{N} \text{ or hyperon production}) \gtrsim 10^{-28} \text{ cm}^2/\text{nucleon} \tag{6-13}$$

Obviously something is strongly inhibiting ψ production in hadron-hadron collisions. Incidently there are no published results on ψ production in pion-nucleon collisions -- the production could be an order of magnitude

higher than in nucleon-nucleon collisions.

There is no substantial data on ψ' production in hadron-hadron collisions.

C. Decay Rate and Decay Modes

The astonishing property of the ψ particles is that their decay rate is relatively small considering their mass. Colliding beams measurements find[50-55] for the decay width

$$\Gamma(\psi) = 69 \pm 15 \text{ KeV} \tag{6-14a}$$

$$\Gamma(\psi) = 400 \begin{smallmatrix} + 400 \\ - 200 \end{smallmatrix} \text{ KeV} \tag{6-14b}$$

As shown in Table II, the established vector mesons -- the hadrons which the ψ particles may most closely resemble -- have decay widths of 4.2 to 150 MeV. Thus the ψ particles have decay widths which are 10 to 1000 times smaller than expected -- hence they are 10 to 1000 times more stable.

As described in detail in the following sections, the ψ predominantly has hadronic decay modes, although 14% of the time it decays to an electron pair or to a muon pair. The ψ could be a hadron; but again there must be some mechanism which inhibits the decay through the strong interactions enough so that the electromagnetic decays are substantial. The ψ' is more complicated since 57% of the time it decays to the ψ. The remaining decays are to hadronic modes -- the electron pair and muon pair decay modes being on the per cent level.

D. Interpretation

Thus the ψ particles seem to be hadrons and yet not quite hadrons. If they are hadrons there is some mechanism which inhibits the strong interactions enough to give:

(a) Relatively narrow decay widths.

(b) Leptonic decay modes.

(c) Relatively small production in hadron-hadron collisions.

There are two types of current theories which have such an inhibition mechanism.[56,57] One possibility is that the ψ's strong decay is exactly forbidden by its possession of a new non-additive quantum number. Various color models are examples of this. The other possibility is that the ψ's strong decay is inhibited by a dynamical principle based on the existence of new additive quantum numbers. Charm is an example of this case in which the ψ's have zero charm quantum number but are composed of charmed quarks.[10,58]

If the ψ's are colored states then presumably they will decay primarily through photon emission. So far we have not seen any strong evidence for radiative decays. The verification of the charm model will probably require the discovery of charmed hadron such as the D and F mesons, with weak decays.[58] Numerous searches are being made for such particles. I will discuss these theories and searches in detail in the spoken lectures, but I will not take the space to write it all down as so much has already been writeen on these theories.

I only note that an extensive search has been made for charmed mesons produced in e^+e^- annihilation at 4.8 GeV.[58] The search looked for narrow peaks in inclusive two and three body state invariant mass distributions in various modes. No significant peaks were found. The results are shown in Table V. The mass region 1.85 to 2.4 is the relevant one for charmed mesons.

To interpret these data we first have to estimate the amount of expected charm meson production. From the usual quark charges, we would estimate that 40% of the events at 4.8 GeV should contain a pair of charmed mesons in addition to any ordinary mesons that may be present. This gives a cross section of about 15 nb for inclusive charmed meson production. There are three types of charmed mesons which will decay weakly. All other charmed mesons will decay into these. Thus, for each type we expect a cross section of about 5 nb. The limits in Table V range from about .1 to .5 nb or from about 2% to 10% in branching ratio.

These limits do not rule out charm models but they made them uncomfortable. Conventional models[57] seem to predict branching ratios into some of these modes from 2 to 5 times higher than the limits.

6.3 Total Cross Section and Masses

Figures 15 and 16 show the apparent cross sections for reactions 6-1 and 6-6 as measured at SPEAR.[50] These are only apparent cross sections because the widths of the resonances are smaller than the experimental resolution.

To obtain apparatus-independent values for the cross sections we integrate over energy to obtain

$$\Sigma_{\psi} = \int \sigma_{\psi}(E)dE = 9900 \pm 1500 \text{ nb} \cdot \text{MeV} \qquad (6\text{-}15)$$

$$\Sigma_{\psi'} = \int \sigma_{\psi'}(E)dE = 3700 \pm 900 \text{ nb} \cdot \text{MeV} \qquad (6\text{-}16)$$

These integrated cross sections are corrected for the rather considerable effect of initial state radiation. The astonishing size of these cross sections relative to the continuum for hadron production is shown in Fig. 6. The masses of the ψ and ψ' as determined at the various laboratories are,

Laboratory	m_ψ (MeV)	$m_{\psi'}$ (MeV)
SLAC (SPEAR)	3095 ± 4	3684 ± 5
DESY (DORIS)	3090 ± 31	3680 ± 37
Frascati (ADONE)	3101 (error not given)	

6.4 Total and Leptonic Widths of the ψ

The ψ has decays into e^+e^- pairs with

$$\frac{\psi \to e^+e^-}{\psi \to \text{all}} = .069 \pm .009 \; ; \tag{6-17}$$

and into $\mu^+\mu^-$ pairs with

$$\frac{\psi \to \mu^+\mu^-}{\psi \to \text{all}} = .069 \pm .009 \tag{6-18}$$

These decay rates together with the total cross section allows us to calculate the true ψ width, as follows.

Assume that the ψ has a Breit-Wigner shape.[6] Then for a decay mode, f, the cross section $\sigma_{\psi,f}$ for the reaction

$$e^+e^- \to \psi \to f \tag{6-19}$$

has an energy dependence similar to that in Eq. 1-22, namely

$$\sigma_{\psi,f} = \frac{\pi(2J + 1)}{s} \frac{4m^2\Gamma_{ee}\Gamma_f}{(s - m^2)^2 + m^2\Gamma} \tag{6-20}$$

Here m is the mass of the ψ, J is its spin, Γ_f is the partial decay width to the state f, and Γ is the total decay width. Going to the non-relativistic form,

$$\sigma_{\psi,f} = \frac{\pi(2J + 1)}{m^2} \frac{\Gamma_{ee}\Gamma_f}{(W - m)^2 + \Gamma^2/4} \tag{6-21}$$

I have ignored radiative effects and interference with the direct channel.

$$e^+e^- \rightarrow f \tag{6-22}$$

Finally, integrating Eq. 6-21 and using J = 1 (see Sec. 6.4), we obtain

$$\Sigma_{\psi,f} = \int \sigma_{\psi,f}\, dW = \frac{6\pi^2}{m^2} \frac{\Gamma_{ee}\Gamma_f}{\Gamma} \quad . \tag{6-23}$$

We can now use Eq. 6-23 to obtain all the widths. In particular,

$$\Gamma_{ee} = \frac{m^2}{6\pi^2} \Sigma_{\psi,\text{all}} \tag{6-24}$$

and

$$\Gamma = \frac{\Sigma_{\psi,\text{all}}}{\Sigma_{\psi,ee}} \Gamma_{ee} \quad . \tag{6-25}$$

Table VI contains the ψ widths as determined at SPEAR.[50] Radiative and interference effects have been included.

6.5 Quantum Numbers of the ψ

Since the ψ is produced in e^+e^- annihilation, our first guesss is that, like the vector mesons, it couples directly to the photon and thus has the same quantum numbers, $J^{pc} = 1^{--}$. This would not have to be the case, however, if the ψ coupled directly to leptons. We can determine the quantum numbers directly by observing the interference between the leptonic decays of the ψ,

$$e^+e^- \to \psi \to e^+e^- \tag{6-26}$$

and

$$e^+e^- \to \psi \to \mu^+\mu^- \tag{6-27}$$

and the direct production of lepton pairs,

$$e^+e^- \to e^+e^- \tag{6-28}$$

and

$$e^+e^- \to \mu^+\mu^- \ . \tag{6-29}$$

How this is done is discussed in Ref. 5. The data[50,55] comfirm the assignment

$$J^{PC} = 1^{--} \text{ for } \psi \tag{6-30}$$

6.6 Hadronic Decays of the ψ

We can determine the isotopic spin of the ψ by observing whether it decays into even or odd numbers of pions (see Eq. 1-14). It turns out that the ψ decays into both even and off numbers of pions -- a violation of I spin. However, this violation occurs in precisely the way we expect it to occur, and in the way it is required to occur, if the ψ couples to a photon.

Consider the three diagrams in Fig. 17. Figures 17(a) shows the direct decay of the ψ into hadrons, (b) shows the decay of the ψ into hadrons via an intermediate photons, and (c) shows the decay into μ pairs. In (b), the nature of the final state, except for a phase factor, must be the same as the non-resonant final state produced in e^+e^- annihilation at the same energy. This state need not conserve isospin and may be quite different from the state produced by (a). Furthermore, we know what contribution (b) must make because the ratio between (b) and (c) must be the same as it would be if the ψ were not in the diagram, about 2.5. Thus, from the data in Table VI, we deduce that if the ψ couples to a photon (a) contributes 68% to the width of the ψ, (b) contributes 18%, and the leptonic modes contribute 14%.

To test this hypothesis we want to compare the ratio of all pion state cross sections to μ pair cross section on and off-resonances. This is done in Table VII.[62] The off-resonance data are from runs at 3.0 GeV. The results are consistent with all of the even number of pion production ($I = 1$) coming from the intermediate photon decay, Fig. 17(b). Most of the odd pion production comes from the direct ψ decay, Fig. 17(a), and the ψ appears to decay directly into a pure $I^G = 0^-$ state.

The study of the decays modes of the ψ is just beginning. The decays that have been identified so far are listed in Table VIII.[59-62] Where the word "seen" is used, it does not imply that the branching ratio is small, but simply that it has not yet been determined.

6.7 Total and Leptonic Widths of the ψ'

The widths of the ψ' can be determined in the same way as those of the ψ were determined (Sec. 6.3). However the analysis is more difficult because the relative leptonic decay rates are smaller. We find for

preliminary values.

$$\Gamma_{ee} = \Gamma_{\mu\mu} \text{ (equality assumed)} \quad 2.2 \pm 0.5 \text{ KeV} \tag{6-31a}$$

$$\Gamma \quad 400 \begin{smallmatrix} + 400 \\ - 200 \end{smallmatrix} \text{ KeV} \tag{6-31b}$$

The width of the ψ' is larger than that of the ψ, but still quite remarkable. This is particularly so since over half of the ψ' decays go to a ψ (Sec. 6.8) leaving only 100-300 KeV for decays to normal hadrons.

6.8 Quantum Numbers of the ψ'

Since the ψ' is produced e^+e^- annihilation, a first guess is again that it has quantum numbers $J^{PC} = 1^{--}$. This guesss is further bolstered by a study of the angular distributions in the $\psi' \to \psi\pi\pi$ decay.

6.9 $\psi' \to \psi$ Decays

The ψ' decays over half the time into the ψ, primarily via the decay mode

$$\psi' \to \psi\pi\pi \ . \tag{6-32}$$

We find[63]

$$\frac{\psi' \to \psi\pi^+\pi^-}{\psi \to \text{all}} = 0.32 \pm 0.04 \ ; \tag{6-33}$$

and

$$\frac{\psi' \to \psi + \text{anything}}{\psi' \to \text{all}} = 0.57 \pm 0.08 \tag{6-34}$$

A values of 0.54 ± 0.10 for this ratio has been reported from DORIS.[61] Hence

$$\frac{\psi' \to \psi + \text{anything}}{\psi' \to \psi\pi^+\pi^-} = 1.78 \pm 0.10 \ .$$

6.10 Other Hadronic ψ' Decays

No other hadronic decays have been identified for the ψ'. This in itself may be significant. We would expect the $42 \pm 8\%$ of the ψ' decays which do not go to ψ's or leptons to go to hadrons in much the same way as the direct ψ decays (see Table VIII). But apparently they go to states with only one missing neutral a much smaller fraction of the time.

7. SUMMARY

We observed four phenomena, each of which in itself is extraordinary:

(a) the ψ particles,

(b) the broad enhancement around 4.1 GeV,

(c) the increase in R from around 2.5 to 5 as W increase through 4 GeV,

(d) the constancy of R above 4.5 or 5 GeV.

Ahead of us lies the fascinating experimental and theoretical tasks of understanding these phenomena. And there is always the haunting question: Are they related or is nature confusing us by crowding unconnected phenomena into a narrow energy range?

References

1. The members of the SLAC-LBL magnetic detector collaboration are SLAC: J.-E. Augustin, A.M. Boyarski, M. Breidenbach, F. Bulos, J.T. Dakin, G.J. Feldman, G.E. Fischer, D. Fryberger, G. Hanson, D.L. Hartill, B. Jean-Marie, R.R. Larsen, D. Lüke, V. Lüth, H.L. Lynch, D. Lyon, C.C. Morehouse, J.M. Paterson, M.L. Perl, T. Pun, P. Rapidis, B. Richter, R.F. Schwitters, W.M. Tanenbaum, F. Vannucci; and LBL: G.S. Abrams, D.D. Briggs, W. Chinowsky, C.E. Friedberg, R. Hollebeek, J.A. Kadyk, G. Goldhaber, A. Litke, B. Lulu, F. Pierre, B. Sadoulet, G. Trilling, J.S. Whitaker, F. Winkelmann, J. Wiss, J.E. Zipse.

2. See for example, V. Silvestrini in Proceedings of the Sixteenth International Conference on High Energy Physics, 1972 (National Accelerator Laboratory, Batavia, Ill., 1973).

3. See for example, J. Lefrancois in Proceedings of the International Symposium on Electron and Photon Interactions at High Energies, 1971 (Laboratory for Nuclear Science, Cornell, 1971).

4. See for example, V.A. Sidorov in Proceedings of the Fourth International Symposium on Electron and Photon Interactions at High Energies, 1969 (Daresbury Nuclear Physics Laboratory, 1969).

5. G.J. Feldman and M.L. Perl, Phys. Repts. C (1975), to be published.

6. M.L. Perl, High Energy Hadron Physics (Wiley, New York, 1974). (The notation in this article follows this book.)

7. N. Cabibbo and R. Gato, Phys. Rev. 124, 1577 (1961).

8. For an example of the use of polarized $e^+ - e^-$ beams to study weak interaction effects in $e^+ - e^-$ interactions see V.K. Cung et al., Phys. Letters 41B, 355 (1972). For discussion of the extent of beam polarization in $e^+ - e^-$ colliding beams facilities see R.F. Schwitters, Nucl. Inst. Methods 118, 331 (1974).

9. C. Llewellyn-Smith and A. Pais, Phys. Rev. D6, 2625 (1972); A. Pais, Phys. Rev. Letters 32, 1081 (1974).

10. For early discussions of charm see J. Bjorken and S.L. Glashow, Phys. Letters 11, 255 (1964); S.L. Glashow et al., Phys. Rev. D2, 1285 (1970); D.B. Lichtenberg, Unitary Symmetry and Elementary Particles, (Academic Press, New York, 1970); M. Gell-Mann, Acta. Phys. Austr. Suppl. IX, 733 (1972); M.Y. Han and Y. Nambu, Phys. Rev. 139, B1006 (1965); for recent discussions see Ref. 57.

11. Y. Frishman, Phys. Reports 13C, 1 (1974); Y. Frishman in Proceedings of the XVI International Conference on High Energy Physics, 1972 (National Accelerator Laboratory, Batavia, Ill., 1972).

12. S. Drell in Proceedings of the XVI International Conference on High Energy Physics, 1972 (National Accelerator Laboratory, Batavia, Ill., 1972).

13. J.J. Sakurai in Proceedings of the Fourth International Symposium on Electron and Photon Interactions at High Energies, 1969 (Daresbury Nuclear Physics Laboratory, Daresbury, England, 1969).

14. J.J. Sakurai, Phys. Letters B46, 207 (1973).

15. M. Greco, Nuc. Phys. B63, 398 (1973).

16. Mass and width values from N. Barash-Schmidt et al., Phys. Letters 50B, No. 1 (1974) which is the 1974 edition of "Particle Properties"; coupling constants from Ref. 3.

17. E. Fermi, Prog. Theoret. Phys. 5, 570 (1950).

18. C. Pelligrini, Ann. Rev. Nucl. Sci. 22, 1 (1972).

19. Proceedings of the IXth International Conference on High Energy Accelerators (Stanford Linear Accelerator Center, Stanford, 1974).

20. J.-E. Augustin et al., Phys. Rev. Letters, 34, 764 (1975).

21. R. Hollebeek, Ph.D. Thesis, University of California at Berkeley, (unpublished); C.C. Morehouse, invited paper presented at the April 1975 meeting of the American Physical Society; and unpublished data of the LBL-SLAC Magnetic Detector Collaboration.

22. M. Bernardini et al., Phys. Letters 51B, 200 (1974), we have used $\sigma_{had}^{(2)}$ from this paper.

23. C. Bacci et al., Phys. Letters 44B, 533 (1973).

24. F. Ceradini et al., Phys. Letters 47B, 80 (1973).

25. A. Litke et al., Phys. Rev. Letters 30, 1189 (1973).

26. G. Tarnopolsky et al., Phys. Rev. Letters 32, 432 (1974).

27. G. Cosme et al., Phys. Letters 40B, 685 (1972).

28. For an alternative explanation using vector meson dominance see G.S. Gournaris and J.J. Sakurai, Phys. Rev. Letters 21, 244 (1968).

29. J. Whitmore, Phys. Reports 10C, 273 (1974).

30. Y. Goldschmidt-Clermont, Acta Phys. Polonica B4, 805 (1973).

31. L.N. Abesalashvli et al., Phys. Letters 52B, 236 (1974).

32. H. Boggild and T. Ferbel, Ann. Rev. Nucl. Phys. 24, 451 (1974).

33. M. Jacob in Proceeding of the Sixteenth International Conference on High Energy Physics, 1972 (National Accelerator Laboratory, Batavia, Ill., 1973).

34. J. Benecke et al., Phys. Rev. 188, 2159 (1969).

35. F.J. Gilman, Phys. Rep. 4C, 95 (1972).

36. J.I. Friedman and H.W. Kendall, Ann. Rev. Nucl. Sci. 22, 203 (1972).

37. A. Bodek et al., in Proceedings of the XVII International Conference on High Energy Physics, 1974 (Science Research Council, Rutherford Laboratory, 1974); and references contained therein.

38. D.J. Fox et al., Phys. Rev. Letter 33, 1504 (1974).

39. S.D. Drell et al., Phys. Rev. D1, 1617 (1970).

40. J.-E. Augustin et al., Phys. Rev. Lett. 33, 1406 (1974).

41. J.J. Aubert et al., Phys. Rev. Lett. 33, 1404 (1974).

42. C. Bacci et al., Phys. Rev. Lett. 33, 1408 (1974).

43. L. Criegee et al., Phys. Lett. 53B, 489 (1975).

44. B. Knapp et al., Phys. Rev. Lett. 34, 1044 (1975).

45. B. Knapp et al., Phys. Rev. Lett. 34, 1040 (1975).

46. J.T. Dakin et al., Phys. Lett. 56B, 405 (1975).

47. L. Cormell et al., Bull. Am. Phys. Soc. 20, 712 (1975).

48. R. Prepost and D. Ritson, (private communications).

49. G.S. Abrams et al., Phys. Rev. Lett. 33, 1453 (1974).

50. A.M. Boyarski et al., Phys. Rev. Lett. 34, 1357 (1975); and unpublished data.

51. W.W. Ash et al., Lett. Nuovo Cimento 11, 705 (1974).

52. R. Baldini Celio et al., Lett. Nuovo Cimento 11, 711 (1974).

53. G. Barbiellini et al., Lett. Nuovo Cimento 11, 718 (1974).

54. R.L. Ford et al., Phys. Rev. Lett. 34, 604 (1975).

55. W. Braunschweig et al., Phys. Lett. 53B, 393 (1974).

56. H. Harari, SLAC report number SLAC-PUB-1514 (unpublished). F.J. Gilman, Proceedings of Orbis Scientiae II, Coral Gables, Florida, (1975) [SLAC report numbers SLAC-PUB-1537].

57. M.K. Gaillard, B.W. Lee, and J.L. Rosner, Rev. Mod. Phys. 47, 277 (1975); M.B. Einhorn and C. Quigg, FNAL report number FERMILAB-Pub-75/21-THY, (to be published in Phys. Rev.).

58. A.M. Boyarski et al., SLAC-PUB-1583 (1975) (submitted to Phys. Rev. Lett.).

59. These data were compiled by B. Jean-Marie of the SLAC-LBL collaboration. I am greatly indebted to him.

60. W. Braunschweig et al., Phys. Lett. 53B, 491 (1975).

61. B. Wiik, Proceedings of the Xth Recontre de Moriond, Meribel-les-Allues, France, 1975.

62. G. Barbiellini et al., Proceedings of the Xth Recontre de Moriond, Meribel-les-Allues, France, 1975.

63. G.S. Abrams et al., Phys. Rev. Lett. 34, 1181 (1975).

TABLE I

The u, d, s are the conventionally accepted quarks, the c separated by the dashed lines is proposed but there is no evidence for its existence comparable to the evidence for the u, d or s. I, I_z, Q, B, Y, S and C are the isotopic spin, z component of the isotopic spin, charge, baryon number, hypercharge, strangeness and charm.

Name	u	d	s	c
Other Name	p	n	λ	p'
I	1/2	1/2	0	0
I_z	+1/2	-1/2	0	0
Q	+2/3	-1/3	-1/3	+2/3
B	1/3	1/3	1/3	1/3
Y	1/3	1/3	-2/3	0
S	0	0	-1	0
C	0	0	0	1

ion.

TABLE II

Properties of Vector Mesons[17]

Name	ρ^0	ω	φ	ρ'
Mass (MeV)	770	783	1020	1600
$I^G(J^P)$	$1^+(1^-)$	$0^-(1^-)$	$0^-(1^-)$	$1^+(1^-)$
Γ(MeV)	150	10.0	4.2	400
Γ_{ee} (KeV)	6.5	0.76	1.34	
Γ_{ee}/Γ	4.3×10^{-5}	7.6×10^{-5}	3.2×10^{-4}	
$\Gamma_{\mu\mu}/\Gamma$	6.7×10^{-5}		2.5×10^{-4}	
$g_V^2/4\pi$	$2.56 \pm .27$	18.4 ± 2.0	11.0 ± 0.9	
hadronic decay modes	$\pi^+\pi^-$ 100%	$\pi^+\pi^-\pi^0$ 90.0% $\pi^0\gamma$ 8.7% $\pi^+\pi^-$ 1.3%	K^+K^- 46.6% K_LK_S 34.6% $\pi^+\pi^-\pi^0$ 15.8% $\eta\gamma$ 3.0%	4π dominant

TABLE III

Parameters of electron-positron colliding beams facilities.

Name	Location	Status	Maximum Total Energy (GeV)	Type
ACO	Orsay	operating	1.1	single ring
ADONE	Frascati	operating	3.1	single ring
DCI	Orsay	under construction	3.6	two rings, four beams
CEA	Cambridge	no longer operating	5.0	rebuilt synchrotron
VEPP-3	Novosibirsk	testing	4.0	single ring
VEPP-4	Novosibirsk	under construction	10. to 14.	single ring
SPEAR	SLAC	operating	~ 9.0	single ring
DORIS	DESY	operating	~ 9.0	two rings
EPIC	Rutherford	proposed	28.0	single ring
PEP	SLAC-LBL	proposed	30.0	single ring
PETRA	DESY	proposed	38.0	single ring

TABLE IV

Values of σ_{had}; R (defined in 1.C) and $\langle N_{ch} \rangle$

Total Energy W(GeV)	σ_{had}(nb)	R	$\langle N_{ch} \rangle$	Ref.	Facility
1.2	218 ± 108	3.6 ± 1.8		22	ADONE
1.3	305 ± 88	5.9 ± 1.7			
1.4	100 ± 70	2.3 ± 1.6			
1.5	148 ± 26	3.8 ± 0.7			
1.6	135 ± 25	4.0 ± 0.7			
1.7	126 ± 18	4.2 ± 0.6			
1.85	73 ± 15	2.9 ± 0.6			
1.9	71 ± 14	3.0 ± 0.6			
1.94	68 ± 21	2.9 ± 0.9			
1.98	53 ± 18	2.4 ± 0.8			
2.1	54.6 ± 3.3	2.77 ± 0.17			
2.4	42 ± 24	2.8 ± 1.6			
2.6	33 ± 14	2.6 ± 1.1			
2.8	18 ± 9	1.6 ± 0.8			
3.0	29 ± 7	3.0 ± 0.7			
1.35	45 ± 18	0.9 ± 0.4		23	ADONE
1.65	36 ± 7	1.1 ± 0.2			
1.98	30 ± 10	1.4 ± 0.5			
2.8	15 ± 3.5	1.4 ± 0.3			
3.0	28 ± 4.5	2.9 ± 0.5			
2.6	18 ± 5	1.4 ± 0.4		24	ADONE
2.8	17 ± 5	1.5 ± 0.5			
3.0	14 ± 5	1.5 ± 0.5			
4.0	26 ± 6	4.7 ± 1.1	4.2 ± 0.6	25	CEA
5.0	21 ± 5	6.0 ± 1.5	4.3 ± 0.6	26	

TABLE IV (continued)

Total Energy W(GeV)	σ_{had}(nb)	R	$\langle N_{ch} \rangle$	Ref.	Facility
2.4	31.8 ± 3.6	2.11 ± 0.24	3.31 ± 0.12		SPEAR
2.6	32.5 ± 4.4	2.53 ± 0.34	3.18 ± 0.15	20	
2.8	29.4 ± 4.1	2.65 ± 0.37	3.37 ± 0.18	21	
3.0	23.3 ± 2.0	2.41 ± 0.21	3.55 ± 0.04		
3.1	22.5 ± 3.4	2.49 ± 0.38	3.51 ± 0.21		
3.2	21.4 ± 2.3	2.52 ± 0.27	3.89 ± 0.12		
3.3	18.9 ± 2.6	2.37 ± 0.33	3.84 ± 0.19		
3.4	18.7 ± 2.4	2.49 ± 0.38	3.93 ± 0.19		
3.6	19.1 ± 2.2	2.85 ± 0.33	4.00 ± 0.17		
3.8	19.7 ± 1.7	3.28 ± 0.28	3.87 ± 0.05		
4.0	24.5 ± 3.3	4.51 ± 0.61	3.90 ± 0.20		
4.1	31.8 ± 3.6	6.15 ± 0.70	4.04 ± 0.17		
4.2	28.1 ± 2.7	5.71 ± 0.55	4.00 ± 0.10		
4.3	23.6 ± 2.8	5.02 ± 0.60	4.02 ± 0.18		
4.4	19.6 ± 2.5	4.37 ± 0.56	4.40 ± 0.24		
4.6	15.3 ± 1.9	3.73 ± 0.46	4.62 ± 0.23		
4.8	18.2 ± 1.5	4.83 ± 0.40	4.31 ± 0.04		
5.0	17.7 ± 1.5	5.09 ± 0.43	4.32 ± 0.09		
5.6	14.7 ± 2.1	5.3 ± 0.8			
6.0	12.0 ± 1.8	5.0 ± 0.7	4.6 ± 0.2		
6.2	12.7 ± 1.9	5.6 ± 0.8	4.3 ± 0.2		
6.8	10.2 ± 1.5	5.5 ± 0.8	4.7 ± 0.3		
7.4	9.4 ± 1.4	5.9 ± 0.9	4.9 ± 0.2		

on
he ψ.

TABLE V

Limits on narrow width resonance production at W = 4.8 GeV
The upper limits are for inclusive cross sections in nb and are at the 90% confidence level.

Decay Mode	Mass Region (GeV/c)		
	1.5 - 1.85	1.85 - 2.4	2.4 - 4.0
$K^{\mp} \pi^{\pm} \pi^{\pm}$	0.51	0.49	0.19
$\pi^{\mp} \pi^{\pm} \pi^{\pm}$	0.48	0.38	0.18
$K_s^o \pi^{\pm}$	0.26	0.27	0.09
$K_s^o K^{\pm}$	0.54	0.33	0.09
$K^{\mp} \pi^{\pm}$	0.25	0.18	0.08
$K_s^0 \pi^+ \pi^-$	0.57	0.40	0.27
$\pi^+ \pi^-$	0.13	0.13	0.09
$K^+ K^-$	0.23	0.12	0.10

TABLE VI

Widths and Branching Ratios of the ψ

Γ_{ee}	4.8 ± 0.6 KeV
$\Gamma_{\mu\mu}$	4.8 ± 0.6 KeV
Γ_{had}	59 ± 14 KeV
Γ	69 ± 15 KeV
Γ_{ee}/Γ	0.069 ± 0.009
$\Gamma_{\mu\mu}/\Gamma$	0.069 ± 0.009
Γ_{had}/Γ	0.86 ± 0.02
Γ_{μ}/Γ_{e}	1.00 ± 0.05

TABLE VII

Comparison of all pion state production to μ pair production at 3.0 GeV and the ψ.

state	$\frac{\sigma^{\psi}_{n\pi}}{\sigma^{\psi}_{\mu\mu}} \Big/ \frac{\sigma^{3.0}_{n\pi}}{\sigma^{3.0}_{\mu\mu}}$
$2\pi^+ 2\pi^-$	0.82 ± 0.22
$2\pi^+ 2\pi^- \pi^0$	> 5.2
$3\pi^+ 3\pi^-$	1.10 ± 0.54
$3\pi^+ 3\pi^- \pi^0$	> 4.5

TABLE VIII

Decay modes of the ψ.
Data from the SLAC-LBL collaboration [59], if no other reference given.

Decay modes identified

mode	comment	%	ref.
e^+e^-		6.9 ± 0.9	
$\mu^+\mu^-$		6.9 ± 0.9	
$p\bar{p}$		0.23 ± 0.05	59,61
$\Lambda\bar{\Lambda}$		seen	
$\eta\gamma$		> 0.15 < 1.8	61 62
$\pi^+\pi^-\pi^o$	Dominantly $\rho\pi$ ($1.3 \pm 0.3\%$)	seen	
$2\pi^+2\pi^-$	Via intermediate γ	0.4 ± 0.1	
$\pi^+\pi^-K^+K^-$		0.5 ± 0.2	
$\pi^+\pi^-p\bar{p}$		seen	
$2\pi^+2\pi^-\pi^o$	Including $\omega\pi\pi$ ($0.8 \pm 0.3\%$) and $\rho\pi\pi\pi$ ($1.2 \pm 0.4\%$) I = 0 implies B. R. ($\pi^+\pi^-3\pi^o$) = 1/2 B. R. ($2\pi^+2\pi^-\pi^o$).	4.0 ± 1.0	
$\pi^+\pi^+\pi^-K_s^oK^-$		seen	
$3\pi^+3\pi^-$	Via intermediate γ	0.4 ± 0.2	
$2\pi^+2\pi^-K^+K^-$		0.3 ± 0.1	
$\pi^+\pi^+\pi^-\pi^oK_s^oK^+$		seen	
$3\pi^+3\pi^-\pi^o$		2.9 ± 0.7	
$4\pi^+4\pi^-\pi^o$		0.9 ± 0.3	

Decay modes searched for and not seen

mode	comment	upper limit %	ref
$\pi^+\pi^-$	G violating	< 0.03	61
K^+K^-		< 0.06	61
$K_s^oK_L^o$		< 0.02	
$\gamma\gamma$	Forbidden for vector meson	< 0.35	60
$\pi^o\gamma$		< 0.55	60,62

Figure Captions

Fig. 1 Hadron production by $e^+ - e^-$ annihilation: (a) the general diagram; (b) the one-photon exchange diagram; (c) the two-photon exchange diagram.

Fig. 2 Kinematics of colliding beams intersecting at: (a) zero angle; and (b) an angle η.

Fig. 3 Feynman diagrams for the reactions: (a) $e^+ + e^- \to \pi^+ + \pi^-$, $e^+ + e^- \to K^+ + K^-$; and (b) $e^+ + e^- \to \mu^+ + \mu^-$.

Fig. 4 The parton model for $e^+ + e^- \to$ hadrons.

Fig. 5 The vector meson dominance model for $e^+ + e^- \to$ hadrons.

Fig. 6 The total cross section, σ_{had}, as a function of $W = \sqrt{s}$. Data sources: below 1.2 GeV, Ref. 16; triangles, Ref. 22; open circles, Ref. 23; squares, Ref. 24; crosses, Refs. 25 and 26; closed circles and ψ data, Refs. 20 and 21.

Fig. 7 (a) σ_{had} versus E_{CM}; (b) $R = \sigma_{had}/\sigma_{\mu\mu}$ versus E_{CM}. References given in caption of Fig. 6, ($E_{CM} = W = \sqrt{s}$).

Fig. 8 (a) The average charged particle multiplicity $\langle N_{ch} \rangle$ for $e^+ + e^- \to$ hadrons; (b) comparison of $\langle N_{ch} \rangle$ with $\langle N_{ch} \rangle$ for hadron-hadron collisions. See text for significance of curves A, B, C. Data from Table IV.

Fig. 9 The single charged particle momentum distribution F(z) versus z where $z = p/p_{max}$. F(z) is normalized to $\int_0^1 F(z)dz = 1$. Data from Ref. 21.

Fig. 10 (a) $\langle p \rangle$ for charged particles versus W; (b) $\langle z \rangle = \langle p/p_{max} \rangle$ for charged particles versus W. Data from Ref. 21.

Fig. 11 A comparison of the observed momentum spectrum for events with three or more charged particles detected at 4.8 GeV to the phase space model using a Monte Carlo calculational method and assuming only pions are produced.

Fig. 12 $E\, d\sigma/d^3p$ for charged particles versus p. Data from Ref. 21.

Fig. 13 Comparison of one-photon exchange diagrams for (a) $e + n \rightarrow e +$ hadrons and (b) $e^+ + e^- \rightarrow$ hadron h + other hadrons.

Fig. 14 $s(d\sigma_{had}/dz)$ for charged particles versus z. Data from Ref. 21.

Fig. 15 The total cross section for $e^+ e^- \rightarrow$ hadrons in the region of the ψ.

Fig. 16 The total cross section for $e^+ e^- \rightarrow$ hadrons in the region of the ψ'.

Fig. 17 Feynman diagrams for (a) the direct ψ decay to hadrons, (b) the ψ decay to hadrons via an intermediate photons, and (c) the ψ decay to μ pairs.

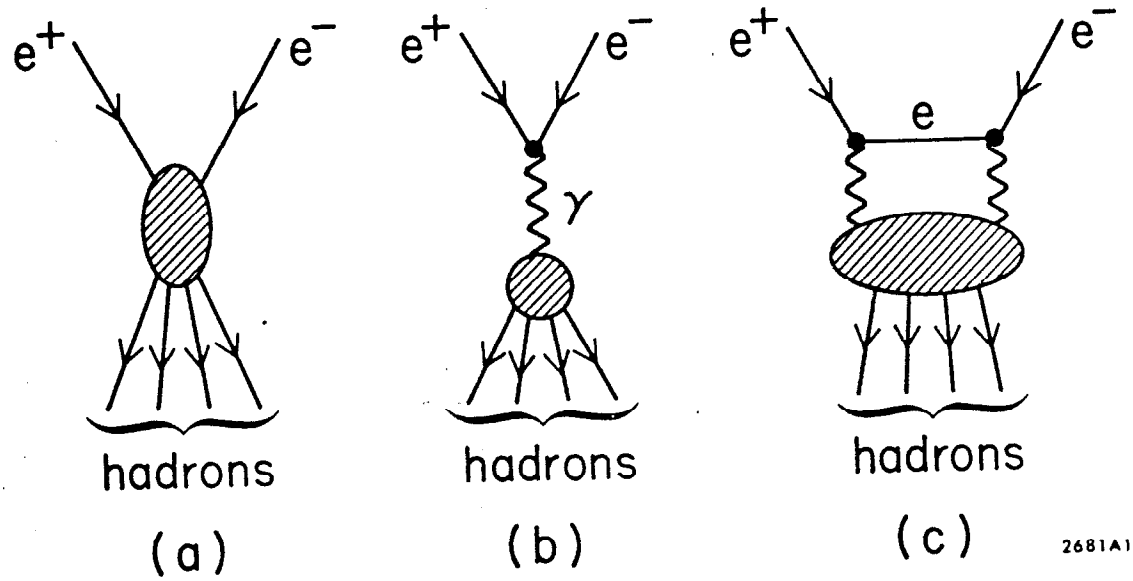
e+
e−
hadrons
(a)
e+
e−
γ
hadrons
(b)
e+
e−
e
hadrons
(c)
2681A1

Fig. 1

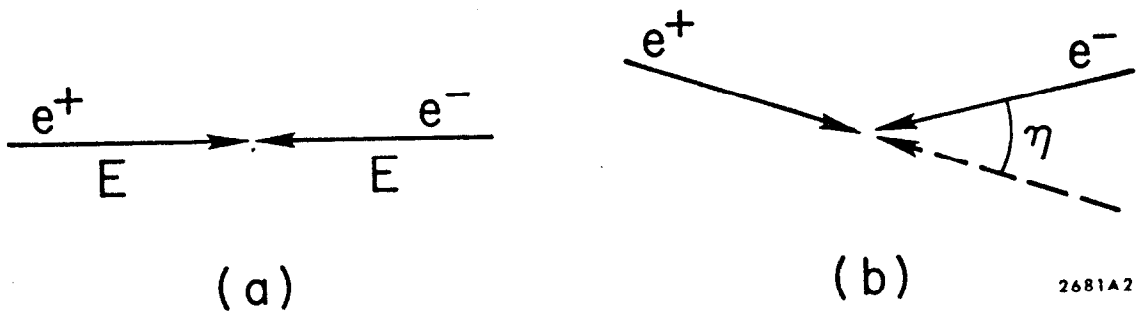
e+
e−
E
E
(a)
e+
e−
η
(b)
2681A2

Fig. 2

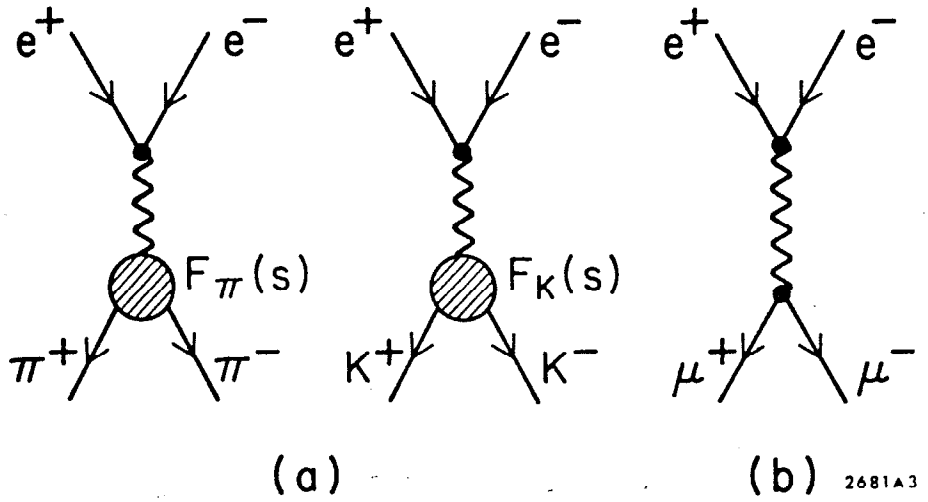
e+
e−
Fπ(s)
π+
π−
e+
e−
FK(s)
K+
K−
e+
e−
μ+
μ−
(a)
(b)
2681A3

Fig. 3

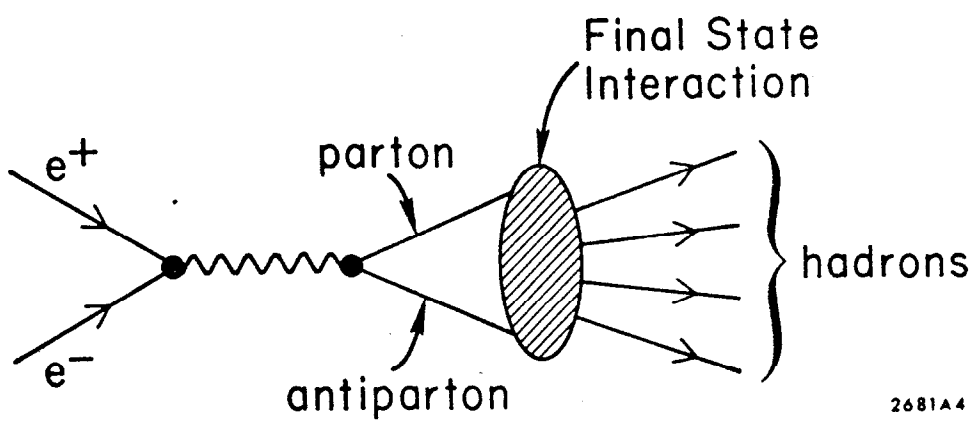
Final State
Interaction
e+
parton
hadrons
e−
antiparton
2681A4

Fig. 4

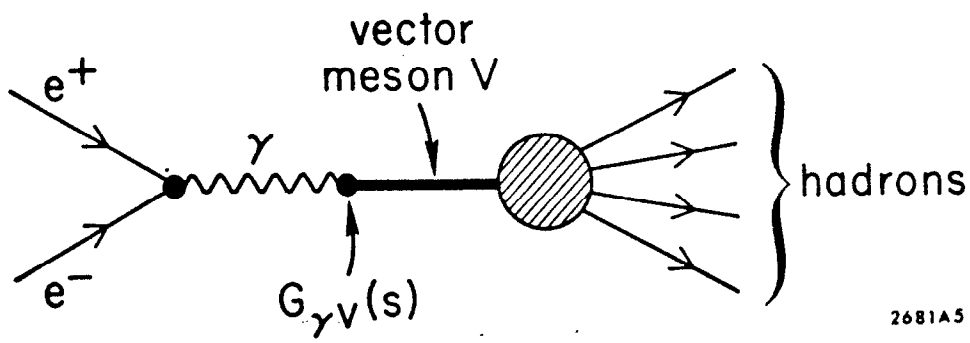
vector
meson V
e+
e−
γ
hadrons
$G_{\gamma V}(s)$
2681A5

Fig. 5

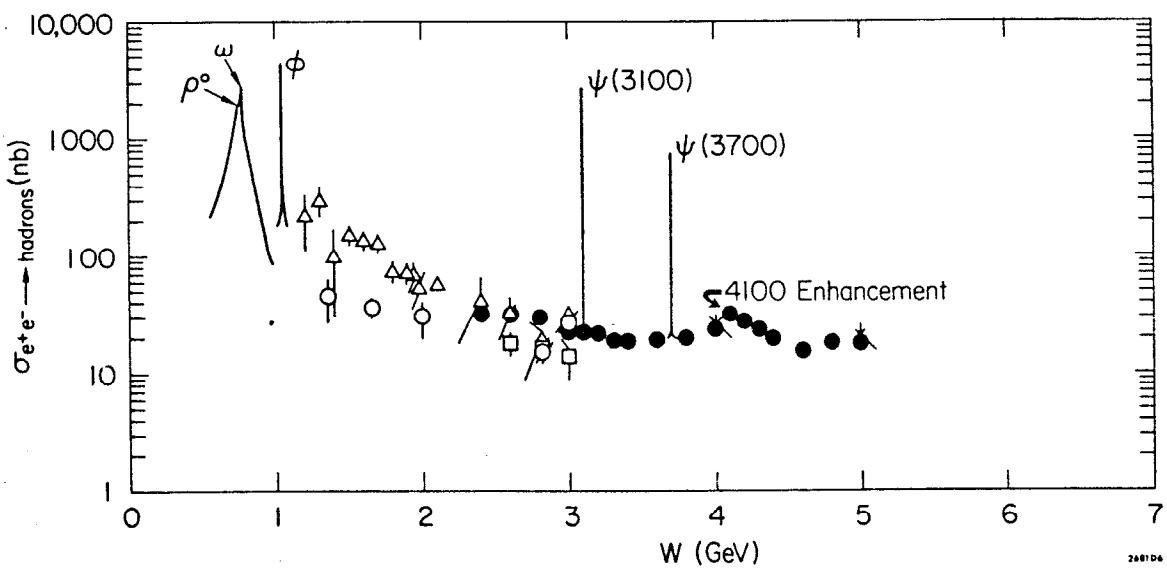
10,000
1000
100
10
1
$\sigma_{e^+e^-\to hadrons}$ (nb)
ρ°
ω
φ
ψ(3100)
ψ(3700)
4100 Enhancement
0
1
2
3
4
5
6
7
W (GeV)

Fig. 6

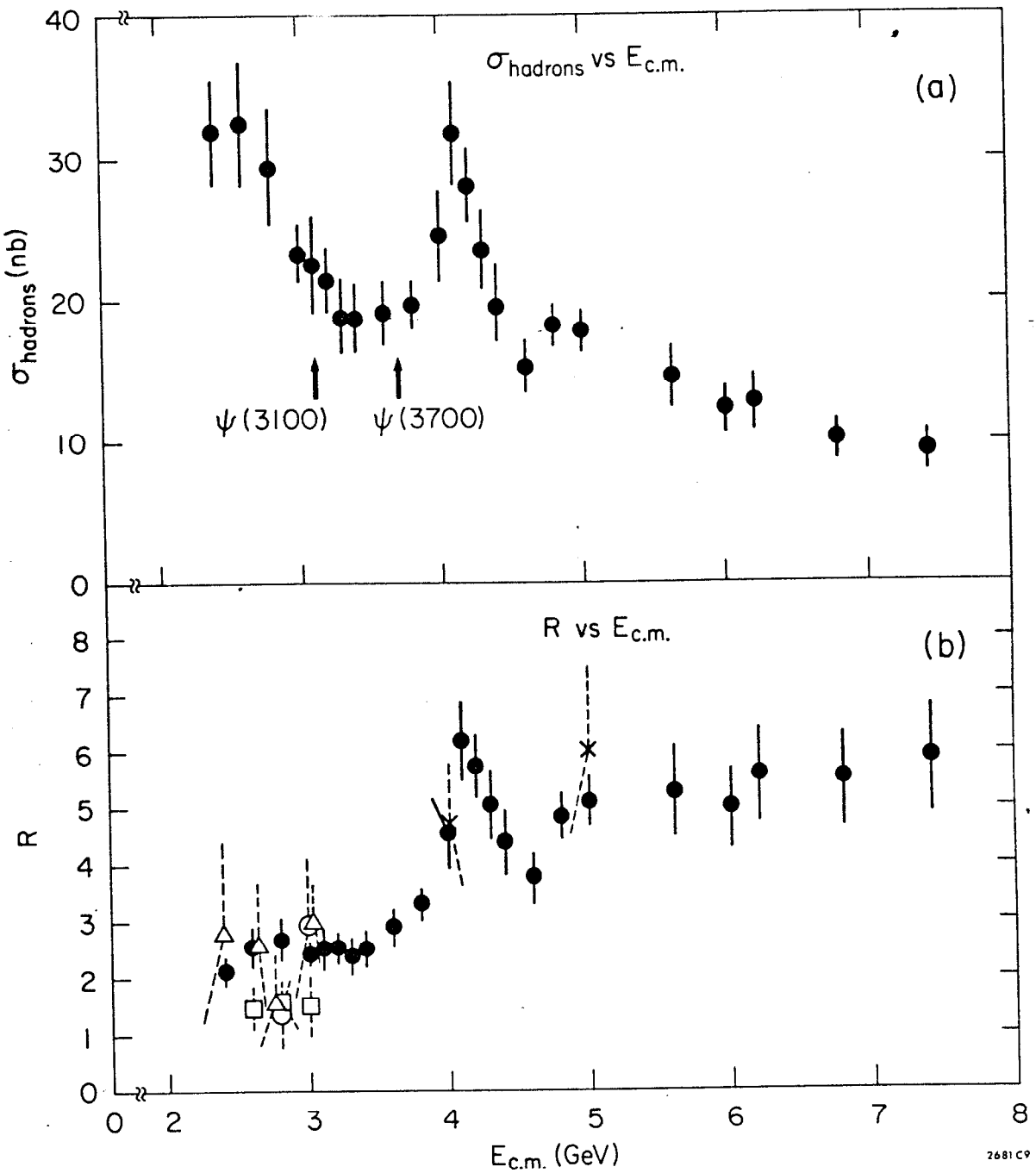
σhadrons vs Ec.m.
(a)
σhadrons (nb)
ψ(3100)
ψ(3700)
R vs Ec.m.
(b)
R
Ec.m. (GeV)
2681C9

Fig. 7

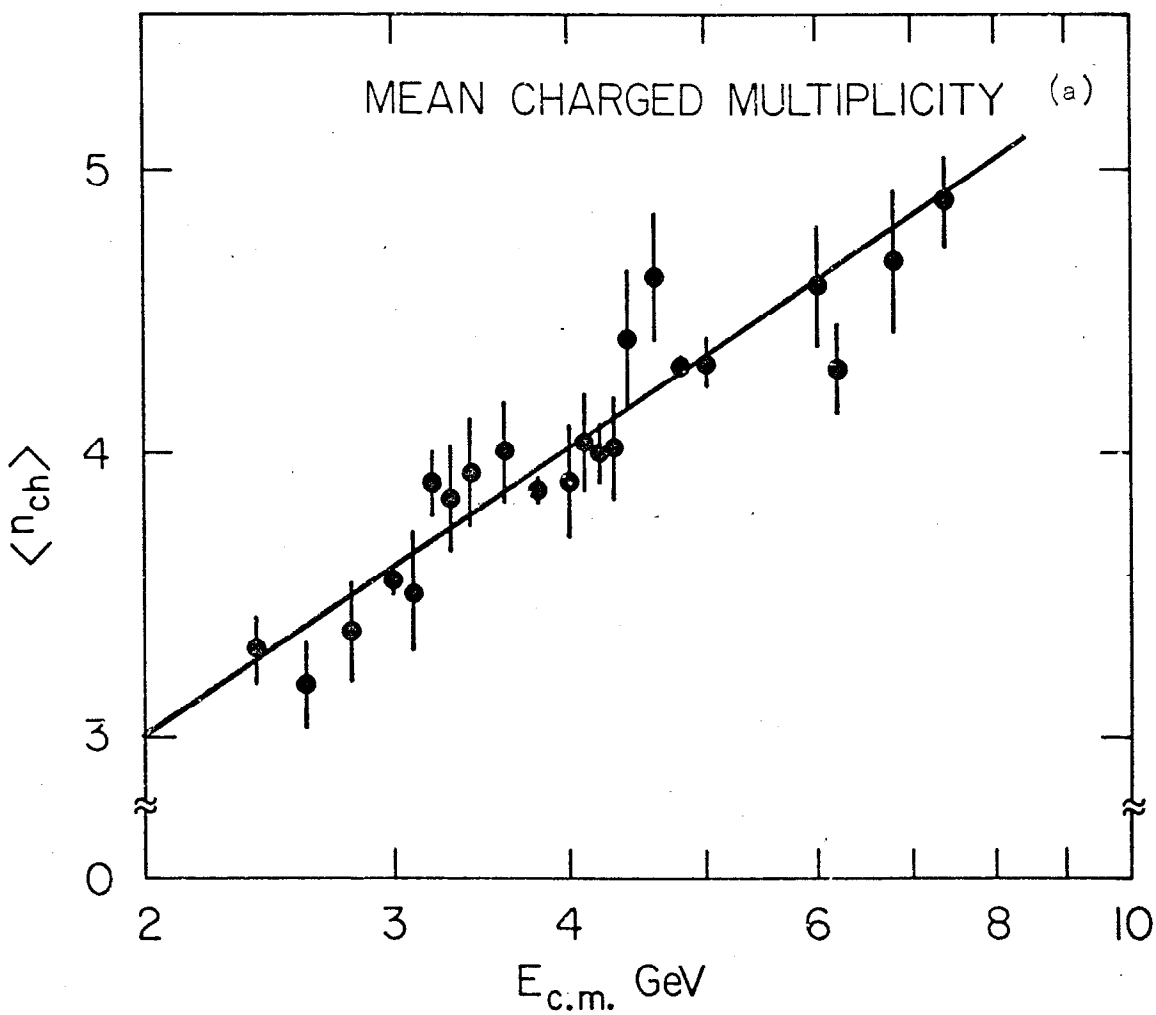

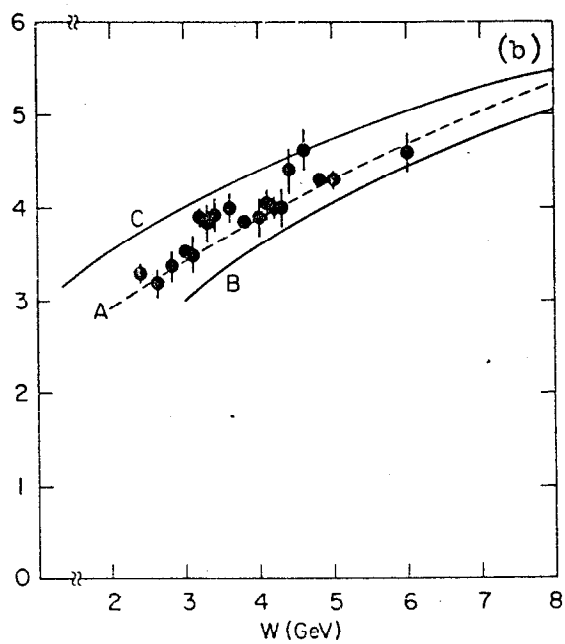

2681A44

Fig. 8

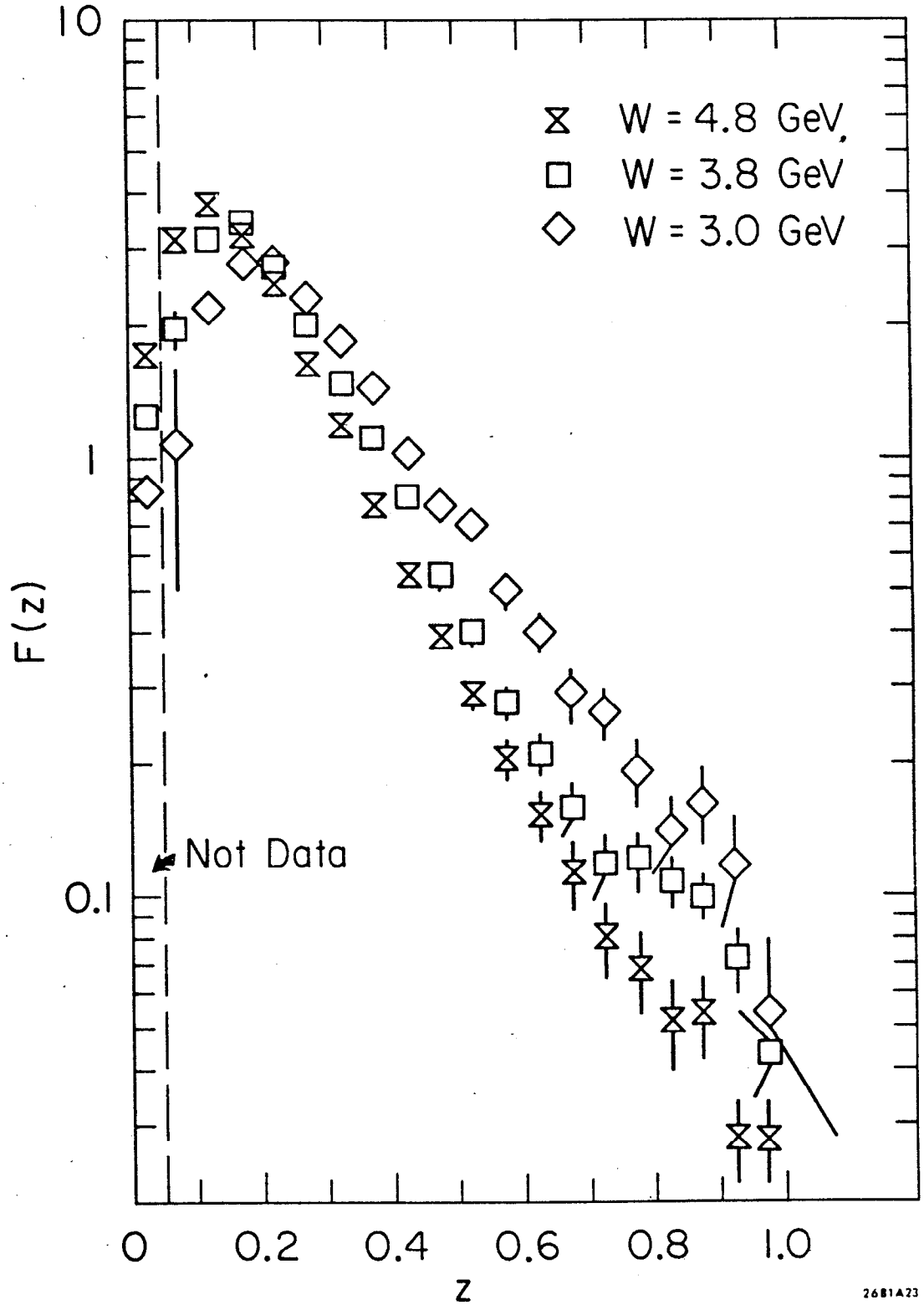
10
1
0.1
F(z)
W = 4.8 GeV
W = 3.8 GeV
W = 3.0 GeV
Not Data
0
0.2
0.4
0.6
0.8
1.0
z
2681A23

Fig. 9

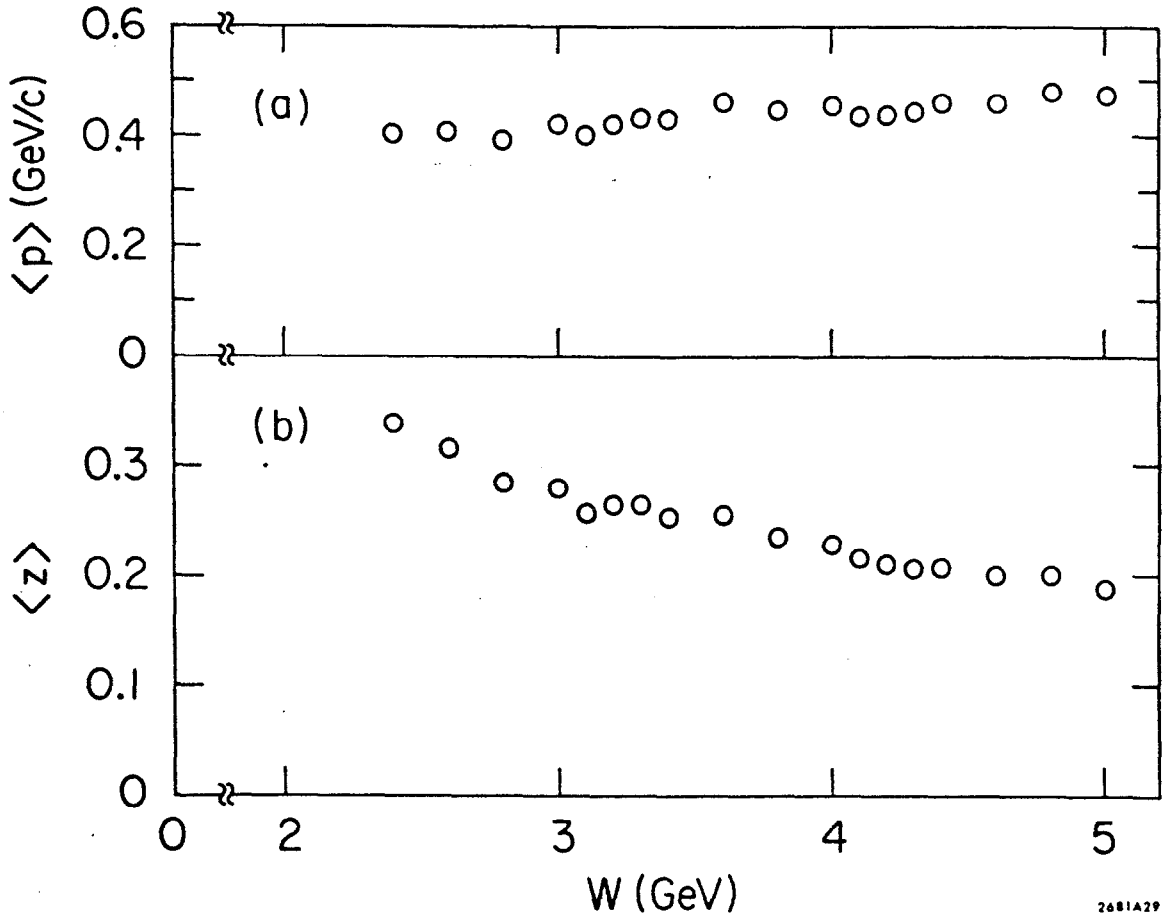

Fig. 10

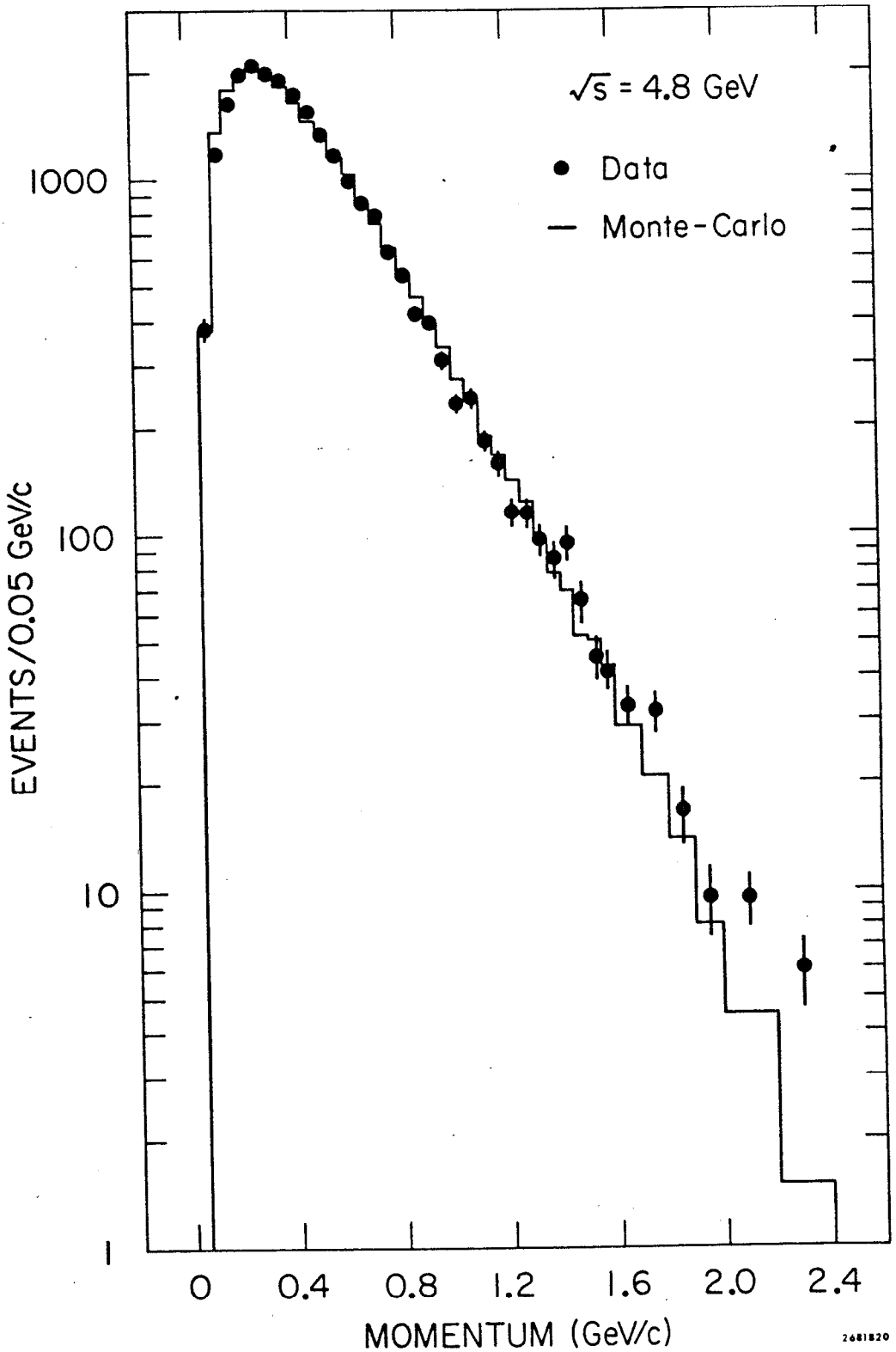
√s = 4.8 GeV
Data
Monte-Carlo
1000
100
10
1
EVENTS/0.05 GeV/c
0
0.4
0.8
1.2
1.6
2.0
2.4
MOMENTUM (GeV/c)
2681B20

Fig. 11

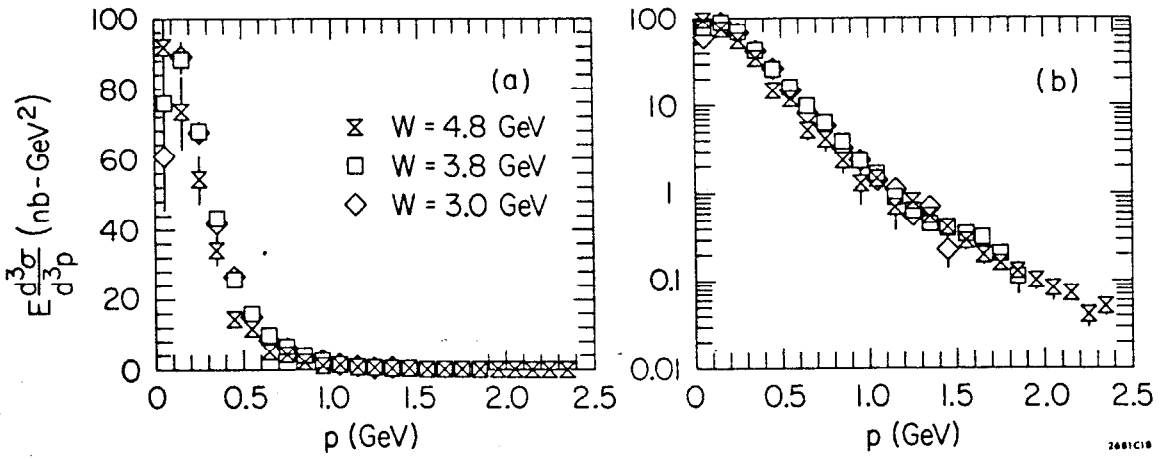
(a)
(b)
W = 4.8 GeV
W = 3.8 GeV
W = 3.0 GeV
$E\frac{d^3\sigma}{d^3p}$ (nb-GeV^2)
p (GeV)
p (GeV)
2681C18

Fig. 12

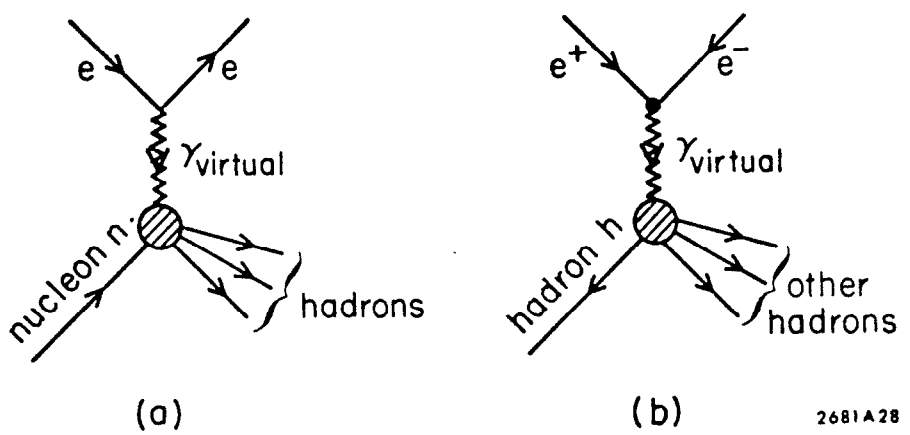
e
e
$\gamma_{virtual}$
nucleon n
hadrons
(a)
e^+
e^-
$\gamma_{virtual}$
hadron h
other hadrons
(b)
2681A28

Fig. 13

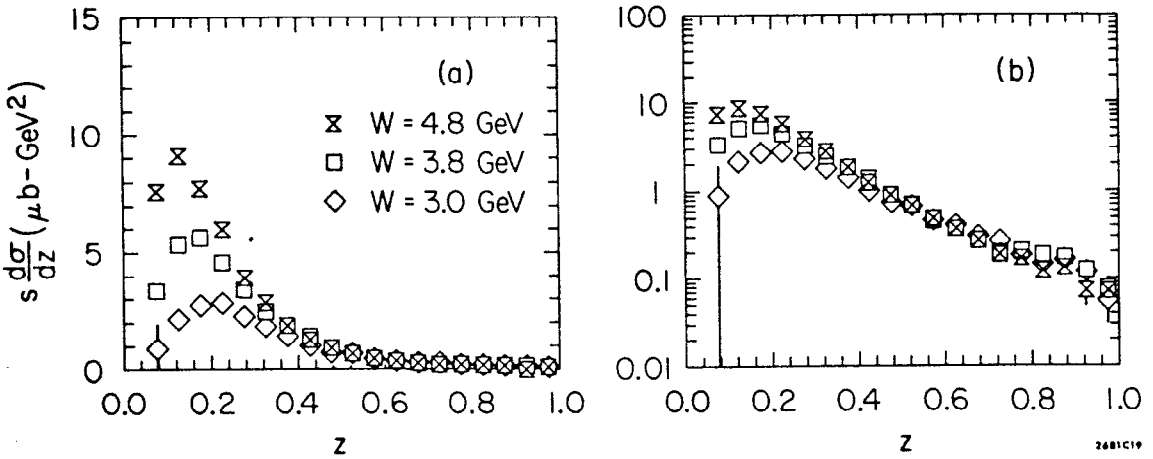
(a)
(b)
W = 4.8 GeV
W = 3.8 GeV
W = 3.0 GeV
$s\frac{d\sigma}{dz}(\mu b\text{-}GeV^2)$
z
z
2681C19

Fig. 14

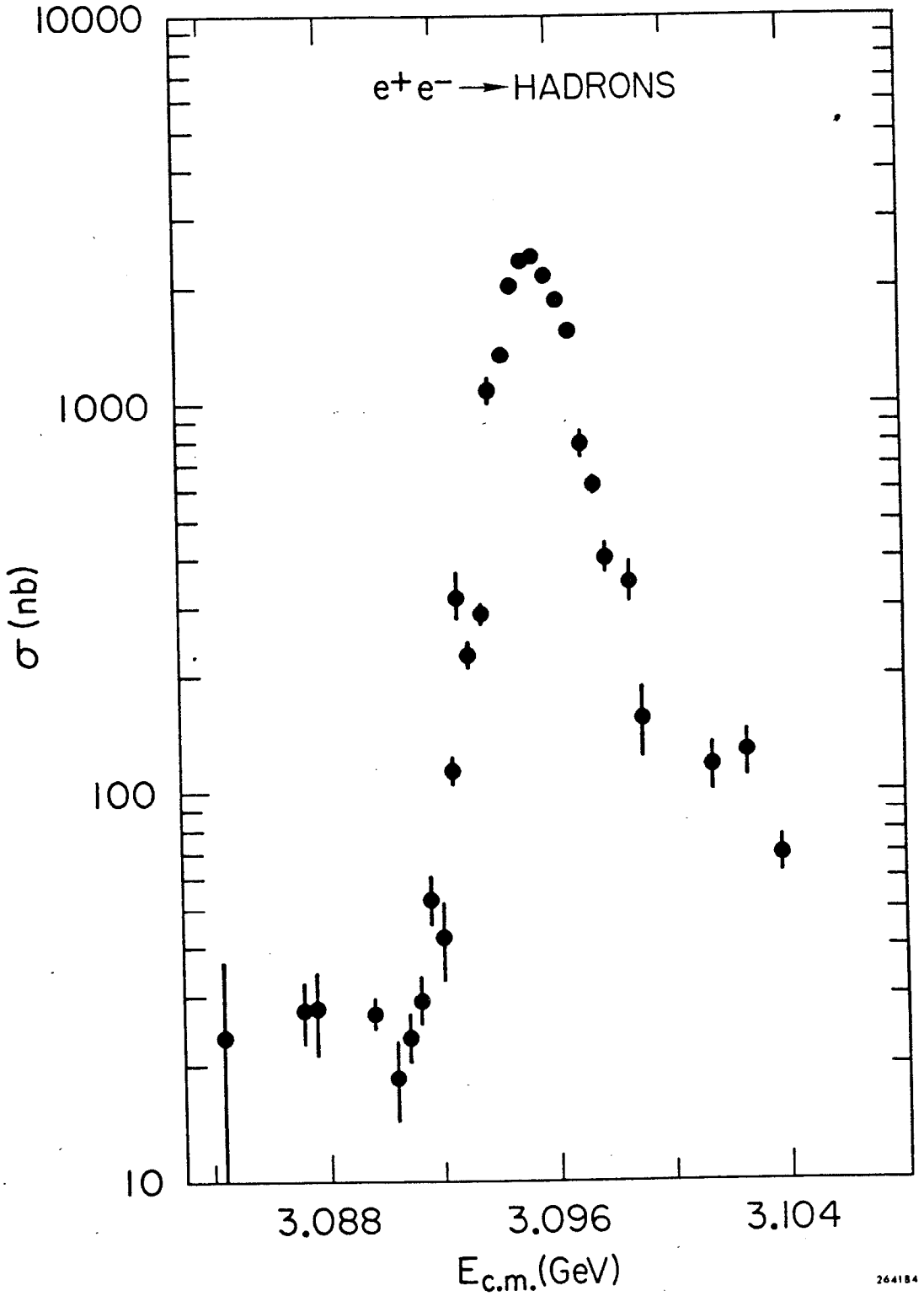
10000
1000
100
10
σ (nb)
e+e− → HADRONS
3.088
3.096
3.104
Ec.m.(GeV)
264184

Fig. 15

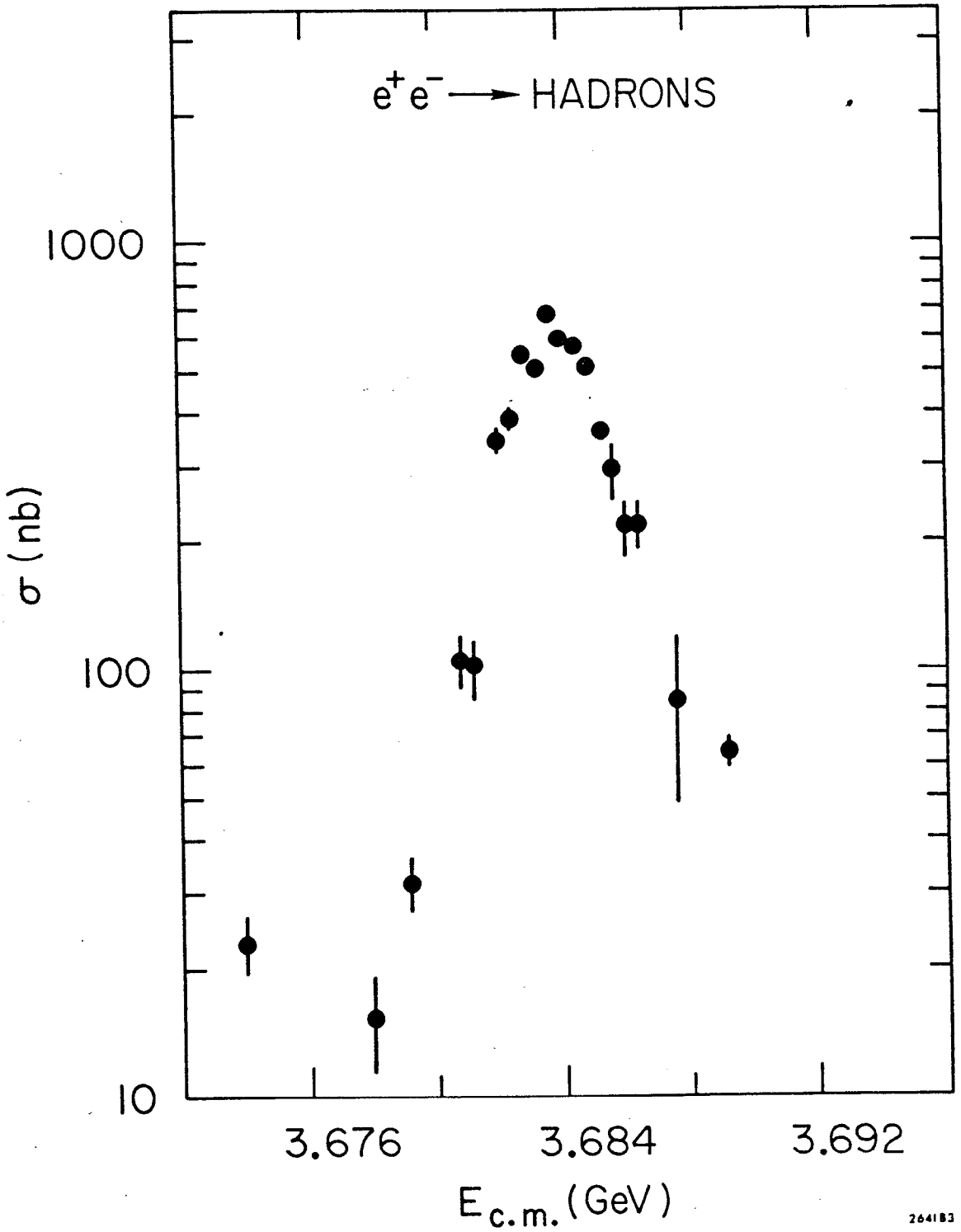
$e^+e^- \longrightarrow$ HADRONS
1000
100
10
σ (nb)
3.676
3.684
3.692
$E_{c.m.}$ (GeV)
2641B3

Fig. 16

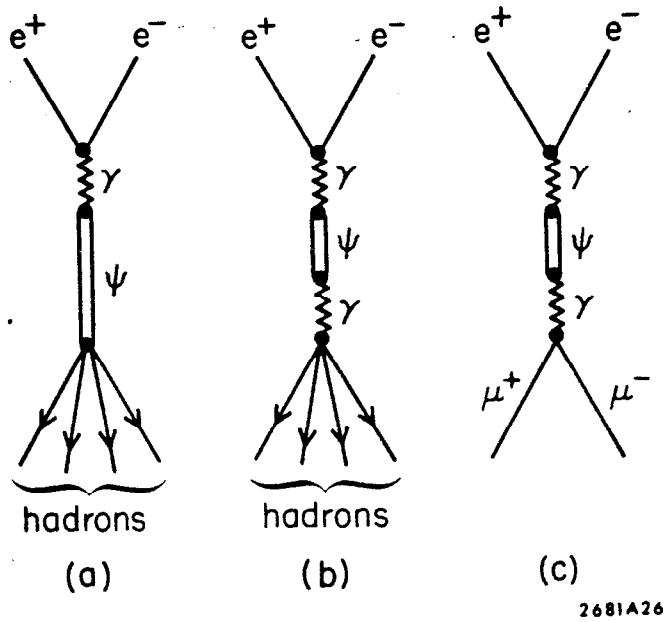

Fig. 17